Strength and morphological behavior of glass-carbon/epoxy hybrid composite plates aging in seawater, engine oil and diesel fuel degradation environment

Ahmet Saylık

a.saylik@alparslan.edu.tr

Mus Alparslan University: Mus Alparslan Universitesi https://orcid.org/0000-0003-1801-0082

Şemsettin Temiz

Inonu Universitesi Muhendislik Fakultesi

Research Article

Keywords: Hybrid composite, woven fiber, impact strength, degradation, aging process, morphological analysis

Posted Date: March 27th, 2024

DOI: https://doi.org/10.21203/rs.3.rs-3967788/v1

Version of Record: A version of this preprint was published at Journal of the Brazilian Society of Mechanical Sciences and Engineering on August 5th, 2024. See the published version at https://doi.org/10.1007/s40430-024-05119-y.

Abstract

In this study, glass/epoxy (GFRP), carbon/epoxy (CFRP) and glass-carbon/epoxy hybrid (GCFRP) composites were aged in seawater, engine oil and diesel fuel degradation environments for 30, 60 and 90 days. The effect of aging environment and time on the structural strength of the composite was examined by applying tensile, three-point bending and low-velocity impact tests to aged composites. SEM analyzes were compared to detect fracture damage occurring in the internal structure of the composites. It was concluded that the degradation environment that most affects the mechanical strength of composites is seawater. Degradation resistance is improved due to the glass/carbon hybridization effect. It has been determined that the glass-carbon hybridization effect in GCFRP composites significantly changes their mechanical strength compared to GFRP and CFRP composites stacked alone. By comparing the glass-carbon hybridization effect in CFRP composites with GFRP and CFRP composites stacked alone, their advantages under different tests are clearly emphasized.

1. Introduction

Fiber Reinforced Plastics (FRPs) are widely used in constantly developing fields such as aerospace, defense and medical industries due to their high specific strength, stiffness and lightness. Fiber-reinforced plastics such as carbon fiber-reinforced plastics (CFRPs) and glass fiber-reinforced plastics (GFRPs) are considered ideal materials, especially in the aerospace industries where high strength-to-weight ratios are more suitable. Exposure of polymer composites to harsh weather conditions often results in structural deterioration, also known as degradation. This can be caused by humidity, seawater or distilled water, hot steam, ultraviolet radiation, and exposure to low or high temperatures [1]. A number of researchers investigated the effects on the mechanical properties of fiber-reinforced polymer matrix composites exposed to different environmental conditions [2–8]. When the flexural behavior of flax and hemp-based hybrid composites exposed to cryogenic environment was examined, it was determined that the flexural stress values of the composites left in the cryogenic environment for 45 minutes decreased by 3.78% [9]. Many studies have been conducted under various environmental conditions to examine the mechanical durability of polymer matrix composites formed through hybridization of carbon and glass fiber with other fiber types. For example, the effect of nanoparticle reinforcement on carbon fiber-reinforced composites was investigated [10–11], and nanoparticle reinforcement was used on glass fiber-reinforced composites to strengthen laminates under environmental aging [12].

Determining the durability of marine vessels designed with reinforced polymer matrix composites in seawater, salt water and similar liquid environments is an important field of study. Composites have been developed and optimized for use in offshore industries [13–18]. When the carbon/flax fiber hybrid composites were aged by applying the high temperature water immersion process, it was determined that the composites with carbon fiber layers on the surface had higher flexural stress and modulus than the composites with flax fiber on the surface [19]. By looking at the behavior of water diffusion in carbon/epoxy composites under static tensile stress, it became clear how the coupling effects between water and mechanical loading of the composites affect the damage development [20]. The fracture

behavior of fiber-reinforced hybrid composites subjected to hydrothermal aging[21] and the changes in their mechanical properties under thermal environmental conditions were investigated comparatively [22–27]. When the effect of moisture absorption of CFRP composites formed with different arrays on damping and dynamic stiffness was examined, it was determined that unidirectional fiber-reinforced composite layers absorbed more water than cross-ply laminates [28]. C-glass braided fiber composites were tested by soaking in a 10 wt.% aqueous H2SO4 (1.89 mol/L) concentration environment at different temperatures and for different durations. As a result, it was concluded that C-glass fibers had more durability in acidic environments than E-glass and carbon fibers [29]. Hybrid rods manufactured with unidirectional carbon/glass (core/shell) pultrusion technology with a diameter of 19 mm were manufactured and immersed in water at different temperatures [30], and in oil wells [31–32], and the relations between shear strength and interface shear strength and degradation times of the rods were examined. When the 3-point bending stress behaviors of glass/carbon/epoxy and 7-layer ply layered composites were studied under different thermal bending loads, it was found that the magnitude of the CTE mismatch between carbon and epoxy was higher than that of glass and epoxy, and the rate of strength and modulus deterioration of composites with more CE layers increased as the test temperature increased [33]. GFRP and CFRP epoxy composites were aged in artificial seawater for 45 days, and it was concluded that the flexural strength of glass/epoxy laminates decreased by about 3.1%, while the flexural strength of carbon/epoxy laminates decreased by 7.7% [34]. In testing the flexural performance of carbon/glass hybrid FRP composite laminates was investigated, $G_2C_4G_2$ was placed symmetrically on the stress and compression sides. It was concluded that composites with $G_2C_4G_2$ array with such two glass layers had approximately 18.3% higher flexural stress than composites with $G_2C_4G_2$ array [35]. A study examining the low-velocity impact (LVI) response of bolted fiber-reinforced polymer joints showed that seawater aging degrades almost 30% of the impact resistance of composite joints, where HNTs reinforced multiscale composite joints exhibited 13% higher impact load performance [36]. In the studies on the impact behavior of the glass-carbon hybridization effect, it has been found that in glass-carbon hybrid layer composites (GCFRP) the impact absorption energy increases by arranging the glass fibers in the upper and lower layers [37], increasing the orientation angle in glass-carbon hybrid pipe composites reduces the impact resistance properties of the material [38] and the effect of impact velocity change applied in glass-carbon hybrid composites on perforated energy were more than different fiber combination changes [39]. When the literature is reviewed on the subject, it is seen that the examination of the damages on and the mechanical properties of glass and carbon fiber reinforced polymer matrix composites after aging them in environments such as freezing-thawing [40], low temperature [41], hydrothermal [42–43], seawater [44–46], alkaline solution [47], and motor oil [48] comes to the fore as recent studies [49]. In this study, after aging of carbon/epoxy, glass/epoxy and glass-carbon epoxy composite laminates in artificial seawater, engine oil and diesel fuel environment for 30, 60 and 90 days, tensile and flexural strength behavior of composite laminates were compared.

2. Materials and Methods

2.1. Materials – reinforcement, resin and composite laminate manufacture

In order to manufacture the composites, 300 gr/m^2 woven type E-glass (twill) fiber and 200 gr/m^2 woven type carbon (plain) fibers were used as reinforcement element as shown in Fig. 1. EPIKOTE epoxy system was used as matrix in composite production (German Lloyd); RIM 135 was used as resin, and RIMH 137 was used as hardener. The mixing ratio of epoxy and hardener was 100:30. Three types of homogeneous layered composites were manufactured by reinforcing epoxy matrix composites with carbon, glass and glass-carbon fibers. For the manufactured composites, fiber fabrics were prepared in 8 layers of 300 ×300 mm sized pieces. The mechanical proper-ties of the glass and carbon fibers used in the study are shown in Table 1. As shown in Fig. 1, GFRP composites consisting of 8 layers of glass fiber, CFRP consisting of 8 layers of carbon fiber, and glass-carbon fiber reinforced hybrid composites (GCFRP) comprised of 2 layers of glass fiber in the top and bottom layers, and 4 layers of carbon in the middle, 8 layers in total, were used. Composite specimens were manufactured using the vacuum assisted resin transfer molding method (VARTM) as shown in Fig. 2. All of the composites left in the vacuum environment were manufactured by being kept at room temperature at 25°C for one day. The fiber volume ratio of glass/epoxy composites (GFRP) was 50.91%, the fiber volume ratio of carbon epoxy composites (CFRP) was 56.06%, and the fiber volume ratio of glass-carbon epoxy hybrid (GCFRP) composites was 54.2%. The thickness of the manufactured glass/epoxy composite sheets (GFRP) was 1.90 ± 0.1 mm, the thickness of the carbon/epoxy composite sheets (CFRP) was 1.85 ± 0.1mm, and the thickness of the glass-carbon epoxy (GCFRP) hybrid epoxy composites was 1.87 ± 0.1 mm.

Table 1
Mechanical and physical properties of materials used as components in composite structures.

Material type	Density (g/cm^3)	Modulus of elasticity (GPa)	Tensile strength (MPa)	Tensilestrain (%)
Carbon fiber	1.79	240	3800	1.6
Glass fiber	2.58	81.50	2306	2.97
Epoxy (RIM 135, RIM H137)	1.19	105	70	12

2.2. Testing methods

2.2.1. Absorption tests

For absorptions tests GFRP, CFRP and GCFRP composite specimens were aged for 30, 60 and 90 days in artificial seawater, engine oil and diesel fuel environments shown in Fig. 3. Artificial seawater environment; In the laboratory, 35 g of salt was added to a beaker and then tap water was added until the

total mass was 1000 g, by mixing until the salt was completely dissolved in the water, an artificial seawater environment was prepared. Shell Helix HX7 10W-40 engine oil was used for the engine oil environment, and Shell V Power diesel fuel was used for the diesel fuel environment. Prior to starting the absorption tests, specimens were conditioned at 23 ◦C and 50% relative humidity for at least seven days before taking the initial dry weight measurement. The liquid absorption of specimens exposed to aging environments was determined by the weight difference between the dry and aged specimens in accordance with ASTM D570-98 [50]. Each specimen was wiped with a clean cloth after the aging period and weighed with a Necklife FA precision balance with 0.1 mg sensitivity. The liquid absorption percentages of the specimens left in different environments were determined by weighing the dry and wet weights of five bending specimens in each sample group. Absorption weight percentile M_t (%) was calculated according to the following equation:

$$M_t\,(\%) = \frac{m_t - m_0}{m_0} \times 100\%$$

1

Here, m_t is the weight of the specimen at t time and m_o was the initial weight of the specimen.

2.2.2. Tensile Test

GFRP and CFRP composites are preferred in structural applications of many different industries. Since the structural strength of these applications is very important; Evaluation of tensile strength, strain and modulus is required. The tensile tests were performed using Shimadzu AGS-X tensile device with a load capacity of 100 kN. The tensile strength and modulus of the composite samples was evaluated according to ASTM D3039-76 standard [51]. The composite samples of dimensions 250 mm (length) × 25 mm (width) were tested. The gauge length of 150 mm and a crosshead speed of 1 mm/min were maintained throughout the test. Epsilon 3542-050M-050-ST axial extensometer with a maximum measurement limit of 50 mm was used to measure the longitudinal elongation precisely. For all aging experimental conditions, five samples of each composite type were tested and the average value was reported. The tensile strength (σ_T), young modulus (E) and strain (ε) are determined by the following expressions:

$$\sigma_T = \frac{P}{A}$$

2

$$\mathrm{E} = \frac{\sigma_T}{\epsilon}$$

3

$$A = w.t$$

4

Here; while *A* represents the surface area of the composite tensile specimen, *w* is the composite sample width and *t* is the composite sample thickness.

2.2.3. Flexural test

The composite plates manufactured with the above-mentioned VARTM technology were cut mechanically with a high-speed computer numerical control (CNC) milling machine, and rectangular bending test specimens of 150 mm (length) $\times$25 mm (width) dimensions were prepared. Following the aging process, the test specimens were taken from the environment, cleaned, wiped and made ready for experimentation. As shown in Fig. 4, five specimens for each composite were tested on the 10 kN capacity Shimadzu AGS- X brand test device for the experiments, and their mean values were reported. The bending test with a span-to-thickness ratio of 32:1 was performed at a constant seater of 1 mm/min at room temperature according to ASTM D7264 [52]. The flexural strength (σ_F), modulus (E_F) and strain to rupture (ε_F) are determined by the following expressions:

$$\sigma_F = \frac{3P_{max}L}{2wt^2}$$

6

$$\mathrm{E}_F = \frac{mL^3}{4wt^3}$$

7

$$\epsilon_F = \frac{6dt}{L^2}$$

8

Here, *L* is the length of the distance between the spans, *w* is the width of the test specimen and *t* is the thickness of the test specimen. P_{max} is the maximum load before fracture, *m* is the slope of the first segment of the load/displacement curve, and *d* represents the maximum bending before fracture.

2.2.4 Low velocity İmpact Test

Composite test samples were cut into 100 x 100 mm^2 dimensions according to the ASTM D7136/D7136M-15 [53] standard and made ready for low-velocity impact tests.

Low-velocity impact testing was performed using the INSTRON 9350 drop tower as shown. A hemispherical impactor with a diameter of 20 mm and mass of m = 1.2 kg was selected for the tests. The weight of the carrier holding the impactor was 4.3 kg. Thus, the total combined load value of the

mass hitting the samples was 5.5 kg. This device allows for different impact energies to be achieved by changing the initial height of the impactor. The diameter of the lower supporting part, to which the samples were fixed, was 76 mm. The samples were placed on this support point and tightened with the clamp to perform the impact tests. The data on the device, the contact force/velocity, and time relationships were recorded by the load cell and then the relationships between time and deflection were obtained by the data collection system (Fig. 5). Impact energy values of 10 J, 20 J, 30 J, and 40 J were applied to each sample type. The results were obtained by repeating the experiment five times for the test applied at each impact energy value.

The impact velocities were 1.907 m/s, 2.697 m/s, 3.303 m/s, and 3.814 m/s and the drop heights were 185 mm, 371 mm, 556 mm, and 742 mm.

3. Results and Discussion

3.1. Environmental Absorption Effect

CFRP, GFRP and GCFRP composite specimens left in an artificial seawater, engine oil and diesel fuel environment were aged for 30, 60 and 90 days. At the end of each aging period, they were cleaned and the absorption weight percentages were calculated. The absorption weight percentages of the composites placed into the artificial seawater environment are shown in Fig. 6 (a), the composites placed in the engine oil are shown in Fig. 6 (b), and the composites placed in the diesel fuel environment are shown in Fig. 6 (c). The mean mass absorption percentage changes with aging of the composites for 90 days are shown in Fig. 7. Average mass absorption of CFRP, GFRP and GCFRP composite specimens in different aging environments for 90 days. In Fig. 6(a), the absorption percentages of composite specimens aged in artificial seawater for 30 days (720 hours) were calculated as 0.201% for GFRP composites, 0.270% for CFRP composites, and 0.244% for GCFRP hybrid composites. Mass absorption percentages of composite specimens aged in artificial seawater for 60 days (1440 hours) were calculated as 0.387% for GFRP composites, 0.551% for CFRP composites and 0.487% for GCFRP hybrid composites. As shown in Fig. 6 (b), the absorption percentages of composite specimens aged in engine oil for 720 hours were calculated as 0.136% for GFRP composites, 0.232% for CFRP composites, and 0.204% for GCFRP hybrid composites. Absorption percentages of composite specimens aged in engine oil for 1440 hours were calculated as 0.470% for GFRP composites, 0.603% for CFRP composites and 0.522% for GCFRP hybrid composites. As shown in Fig. 6(c), the absorption percentages of composite specimens aged in diesel fuel for 720 hours were calculated as 0.106% for GFRP composites, 0.206% for CFRP composites, and 0.155% for GCFRP hybrid composites. Absorption percentages of composite specimens aged in diesel fuel for 1440 hours were calculated as 0.354% for GFRP composites, 0.446% for CFRP composites and 0.386% for GCFRP hybrid composites.

In Fig. 7, the mean mass absorption percentages of the composite specimens that were aged in artificial seawater, engine oil and diesel fuel for 90 days (2160 hours) were calculated. It was observed that the mean absorption percentage of GCFRP composites was higher than the mean absorption percentage of

GFRP composites, and lower than the mean absorption percentage of CFRP composites in all aging environments. The difference between the percentage of mass absorption values in all of the composite specimens was calculated between 720 hours and 1440 hours. When the effects of the environments on the absorption values were examined, it was determined that the highest values were in the machine oil environment, and the lowest absorption values were in the diesel fuel environment.

3.2. Tensile Strength

The mechanical properties obtained as a result of the tensile test of composite samples aged for 30, 60 and 90 days in seawater (RO), engine oil (EO) and diesel fuel (FO) aging conditions are presented in Table 2. The elasticity modulus of GFRP composites at room conditions was calculated as 27.10 GPa and the maximum tensile stress was 503.208 MPa, the elasticity modulus of the CFRP composite was calculated as 61.62 GPa and the maximum tensile stress was 804.306, the maximum tensile stress of the GCFRP hybrid composite was calculated as 603.814 MPa and the elasticity modulus was 40.28 GPa.

Table 2
Tensile strength of composites aged in seawater, engine oil and diesel fuel.

Aging Environment	Composite Type	Young's Modulus (GPa)	Tensile Strength (MPa)	Elongation at Break (%)
Room Conditions	GFRP	27.10	503.208	0.052
Room Conditions	CFRP	61,62	804.306	0.044
Room Conditions	GCFRP	40,28	603.814	0.042
SW-30 Day Aging	GFRP	25.04	475.157	0.055
SW-30 Day Aging	CFRP	57.30	743.867	0.043
SW-30 Day Aging	GCFRP	38.14	550.870	0.042
SW-60 Day Aging	GFRP	23.52	422.659	0.053
SW-60 Day Aging	CFRP	51.68	683.867	0.043
SW-60 Day Aging	GCFRP	36.57	498.363	0.045
SW-90 Day Aging	GFRP	22.49	359.985	0.050
SW-90 Day Aging	CFRP	51.53	654.267	0.043
SW-90 Day Aging	GCFRP	36.08	488.154	0.045
EO-30 Day Aging	GFRP	23.58	474.074	0.053
EO-30 Day Aging	CFRP	55.04	715.143	0.044
EO-30 Day Aging	GCFRP	38.84	583.903	0.043
EO-60 Day Aging	GFRP	23.07	468.852	0.050
EO-60 Day Aging	CFRP	53.35	675.742	0.044
EO-60 Day Aging	GCFRP	38.66	564.425	0.044
EO-90 Day Aging	GFRP	22.77	458.444	0.050
EO-90 Day Aging	CFRP	52.82	664.545	0.045
EO-90 Day Aging	GCFRP	37.92	520.667	0.042
DO-30 Day Aging	GFRP	23.95	497.339	0.053
DO-30 Day Aging	CFRP	57.66	728.377	0.042
DO-30 Day Aging	GCFRP	39.19	589.667	0.042
DO-60 Day Aging	GFRP	23.47	472.470	0.053

Aging Environment	Composite Type	Young's Modulus (GPa)	Tensile Strength (MPa)	Elongation at Break (%)
DO-60 Day Aging	CFRP	54.05	690.497	0.045
DO-60 Day Aging	GCFRP	38.90	580.173	0.042
DO-90 Day Aging	GFRP	22.49	435.306	0.050
DO-90 Day Aging	CFRP	53.03	628.855	0.045
DO-90 Day Aging	GCFRP	38.33	550.296	0.045

Stress-strain graphs of GFRP, CFRP and GCFRP composites aged for 90 days in seawater environment (Fig. 8), engine oil (Fig. 9) and diesel oil environment (Fig. 10) are shown. It was concluded that the modulus of elasticity values of GFRP, CFRP and GCFRP composites at room temperature conditions decreased by 17.01% in GFRP composites, 16.37% in CFRP composites, and 10.42% in GCFRP composites after aging in artificial seawater for 90 days. It was concluded that the modulus of elasticity values of GFRP, CFRP and GCFRP composites at room temperature conditions decreased by 15.97% in GFRP composites, 14.28% in CFRP composites and 5.85% in GCFRP composites after aging in engine oil environment for 90 days. It was concluded that the modulus of elasticity values of GFRP, CFRP and GCFRP composites at room temperature conditions decreased by 17.1% in GFRP composites, 13.94% in CFRP composites and 4.84% in GCFRP composites after aging in diesel fuel environment for 90 days (Fig. 11)

3.3 Flexural Strength

The mechanical properties obtained as a result of the three-point bending test of composite samples aged for 30, 60 and 90 days in seawater (RO), engine oil (EO) and diesel fuel (FO) aging conditions are presented in Table 3.

Table 3
Flexural strength of composites aged in seawater, engine oil and diesel fuel.

Aging environment	Composite type	Flexural Modulus (GPa)	Flexural Strength (MPa)	Flexural Strain (mm/mm)
Room Conditions	GFRP	22.919	547.964	0.03512
Room Conditions	CFRP	43.157	721.410	0.01667
Room Conditions	GCFRP	23.776	544.388	0.03007
SW-30 Day Aging	GFRP	21.077	483.167	0.03146
SW-30 Day Aging	CFRP	42.450	620.343	0.01505
SW-30 Day Aging	GCFRP	23.084	504.309	0.02643
SW-60 Day Aging	GFRP	19.884	457.734	0.02952
SW-60 Day Aging	CFRP	40.482	579.908	0.01389
SW-60 Day Aging	GCFRP	21.772	490.076	0.02579
SW-90 Day Aging	GFRP	19.682	447.538	0.02785
SW-90 Day Aging	CFRP	39.092	532.504	0.01375
SW-90 Day Aging	GCFRP	21.512	449.312	0.02476
EO-30 Day Aging	GFRP	20.796	537.366	0.03388
EO-30 Day Aging	CFRP	42.630	626.090	0.01610
EO-30 Day Aging	GCFRP	22.992	518.076	0.02852
EO-60 Day Aging	GFRP	20.140	525.832	0.03240
EO-60 Day Aging	CFRP	40.598	593.779	0.01552
EO-60 Day Aging	GCFRP	21.979	499.299	0.02795
EO-90 Day Aging	GFRP	19.790	502.135	0.03209
EO-90 Day Aging	CFRP	38.439	579.526	0,01552
EO-90 Day Aging	GCFRP	21.494	483.620	0.02642
DO-30 Day Aging	GFRP	21.389	544.587	0.03497
DO-30 Day Aging	CFRP	42.524	668.366	0.01645
DO-30 Day Aging	GCFRP	22.105	536.638	0.02848
DO-60 Day Aging	GFRP	19.996	535.425	0.03430

Aging environment	Composite type	Flexural Modulus (GPa)	Flexural Strength (MPa)	Flexural Strain (mm/mm)
DO-60 Day Aging	CFRP	40.660	626.056	0.01504
DO-60 Day Aging	GCFRP	21.978	514.342	0.02747
DO-90 Day Aging	GFRP	19.759	522.575	0.03388
DO-90 Day Aging	CFRP	39.016	605.960	0.01481
DO-90 Day Aging	GCFRP	21.621	491.250	0.02723

The flexural stress- flexural strain performances of GFRP, CFRP and GCFRP composites aged in artificial seawater environment, engine oil environment, and diesel fuel environment are shown in Fig. 12, Fig. 13, and Fig. 14, respectively. The flexural modulus of GFRP composites at room conditions was calculated as 22.919 GPa and the maximum flexural stress was 547.964 MPa, the flexural modulus of the CFRP composite was calculated as 43.157 GPa and the maximum flexural stress was 721.410, the maximum flexural stress of the GCFRP hybrid composite was calculated as 544.388 MPa and the flexural modulus was 23.776 GPa.

When the effect of aging of GFRP composites for different time periods and in different environmental conditions on the flexural behavior was examined, it was seen that as the aging time increased in artificial seawater environment as shown in Fig. 12 (a), and the gap between the stress-strain curves decreased significantly compared to the engine oil environment (Fig. 12 (b)) and diesel fuel environment (Fig. 12 (c)) flexural stress-strain curves. When the effect of aging of CFRP composites for different time periods and in different environmental conditions on the flexural behavior was examined, it was clearly seen in Fig. 13 (b) that the gap between the stress-strain curves with the increase of the aging time in the oil environment was higher compared to the aging in the artificial seawater environment (Fig. 13 (a)) and diesel fuel environment (Fig. 13 (c)). When the effect of aging of GCFRP hybrid composites for different time periods and in different environ-mental conditions on the flexural behavior was examined, it was determined that the gap between the curves of the flexural stress-strain curve in the artificial seawater environment shown in Fig. 14 (a) was more pronounced than the engine oil aging (Fig. 14 (b)) and diesel fuel environment (Fig. 14 (c)).

The mean flexural strengths and flexural modulus of the data obtained from the stress-strain curves of the composites aged for 90 days in different environments are shown in Fig. 15.

It was calculated that the flexural stress strengths of GFRP composites at room conditions decreased by 16.58% with aging in artificial seawater environment, by 5.95% in engine oil, and by 5.83% in diesel fuel environment. And the flexural stress strengths of CFRP composites at room conditions decreased by 14.01% with aging in artificial seawater environment, by 16.86% in engine oil, and by 12.20% in diesel fuel environment. The flexural stress strengths of GCFRP hybrid composites at room conditions decreased

by 12.59% with aging in artificial seawater environment, by 9.12% in engine oil, and by 6.62% in diesel fuel environment (Fig. 15). Figure 16 shows the damages that occurred on the compo-sites after the three-point bending test. The specimens started to fracture after bending along the loading pin. Fiber fracture and delamination occurred depending of the region where bending damage occurred.

3.4. İmpact strength

Low- velocity impact tests in normal environment (room temperature) were carried out by weight drop tests at four different impact energies, and 10 J, 20 J, 30 J and 40 J impact tests were applied to estimate the penetration and perforation energy values of GFRP, CFRP and GCFRP composites [AS]. Contact force, deflection (displacement) and absorbed energy values of the composites subjected to low velocity impact tests at four different energy levels are shown in Table 4.

Table 4
Low-velocity impact behavior of GFRP, CFRP and GCFRP composites according to changing impact energy.

Composite type	Impact energy (J)	Impact velocity (m/s)	Contact force (N)	Deflection (displacement) (mm)	Absorbed energy (J)
GFRP	10	1.907	4795.705	3.995	4.726
	20	2.967	5847.293	6.219	16.973
	30	3.303	7210,891	8.829	27.479
	40	3.814	7361.118	13.210	37.386
CFRP	10	1.907	3674.781	4.344	6.901
	20	2.967	4137.018	8.893	19.233
	30	3.303	4888.152	12.328	25.737
	40	3.814	4737.925	12.244	25.496
GCFRP	10	1.907	4402.804	3.954	5.834
	20	2.967	5292.609	7.735	17.672
	30	3.303	5939.741	11.772	29.794
	40	3.814	6332.642	14.811	35.814

As shown in Fig. 20, 4 different energy values were applied to estimate the penetration and perforation energy values of these composites.

Figure 17 (a) shows the absorbed energy-time curves of the GFRP composite laminates, Fig. 17 (b) shows the absorbed energy-time curves of the CFRP composite laminates, and Fig. 17 (c) shows the

absorbed energy-time curves of the GCFRP composite laminates. Figure 18 respectively shows the equal energy profile diagrams of the GFRP, CFRP, and GCFRP composites.

The damages occurring on the back surfaces of CFRP, GFRP and GCFRP composites tested at low-velocity impact energies of 10 joules, 20 joules, 30 joules and 40 joules after the impact test are shown in Fig. 19.

In the absorbed energy-impact energy graph of GFRP, CFRP and GCFRP composites in Fig. 17, it was determined that the absorbed energy value of GFRP and GCFRP composites increased up to 40 J, while the absorbed energy value of CFRP composite decreased after 30 J. At the threshold of these data, it was decided to apply low-velocity impact tests at 30 J impact energy to all composites taken from aging environments, as it was predicted that the impact durability would decrease when the three composite types were placed in aging environments. Contact force, collapse and absorbed energy values at 30 J impact energy of GFRP, CFRP and GFRP composites aged in seawater, engine oil and diesel fuel environment are shown in Table 5.

Table 5
Low-velocity impact strength of GFRP, CFRP and GCFRP aged composites at 30 J impact energy.

Aging environment	Composite type	Contact Force (N)	Deflection (mm)	Absorbed Energy (J)
Room Conditions	GFRP	7210.891	8.829	27.479
Room Conditions	CFRP	4888.152	12.328	25.737
Room Conditions	GCFRP	5939.741	11.772	29.794
SW-30 Day Aging	GFRP	6864.651	9.1239	27.238
SW-30 Day Aging	CFRP	3189.432	12.300	14.219
SW-30 Day Aging	GCFRP	5465.948	11.858	26.804
SW-60 Day Aging	GFRP	4807.261	10.498	28.137
SW-60 Day Aging	CFRP	3131.653	10.659	13.794
SW-60 Day Aging	GCFRP	3975.235	15.390	24.432
SW-90 Day Aging	GFRP	4680.146	12.317	29.595
SW-90 Day Aging	CFRP	2634.748	9.713	12.279
SW-90 Day Aging	GCFRP	3813.452	16.608	24.239
EO-30 Day Aging	GFRP	6829.549	9.272	26.078
EO-30 Day Aging	CFRP	3351.215	12.304	23.025
EO-30 Day Aging	GCFRP	5789.514	11.805	28.630
EO-60 Day Aging	GFRP	5119.270	12.441	26.309
EO-60 Day Aging	CFRP	3154.765	12.038	22.145
EO-60 Day Aging	GCFRP	5026.823	12.417	28.062
EO-90 Day Aging	GFRP	4807.261	10.506	26.998
EO-90 Day Aging	CFRP	3027.650	11.506	17.290
EO-90 Day Aging	GCFRP	4495.251	13.223	27.720
DO-30 Day Aging	GFRP	6933.549	9.642	27.772
DO-30 Day Aging	CFRP	3674.781	12.866	23.459
DO-30 Day Aging	GCFRP	5708.622	10.607	29.510
DO-60 Day Aging	GFRP	5639.287	9.592	27.594

Aging environment	Composite type	Contact Force (N)	Deflection (mm)	Absorbed Energy (J)
DO-60 Day Aging	CFRP	3143.209	12.723	23.203
DO-60 Day Aging	GCFRP	4957.488	11.814	29.823
DO-90 Day Aging	GFRP	5142.382	9.606	27.510
DO-90 Day Aging	CFRP	3085.429	12.674	22.602
DO-90 Day Aging	GCFRP	3963.679	13.389	26.736

GFRP, CFRP and GCFRP composites, which were impact tested at 30 J impact energy and aged in seawater, engine oil and diesel fuel environment for 90 days, respectively; contact force-deflection graphs are shown in Fig. 20. The maximum contact forces obtained from the impact behavior of GFRP, CFRP and GCFRP composites aged for 30, 60 and 90 days are shown in Fig. 21 and the maximum deflection(displacement) values are shown in Fig. 22.

In aged composites; With the increase of aging time, GFRP composites transitioned from penetration to perforation and the energy values absorbed became close to the full penetration energy. In CFRP composites, due to the aging effect, complete perforation occurred more clearly and the absorbed energy values decreased. GCFRP composites, like GFRP composites, started to perforate as the aging times increased, and their absorbed energy decreased (Table 2).It was concluded that the environment that most reduced the maximum contact force values of glass/epoxy (GFRP), carbon/epoxy and glass-carbon/epoxy (GCFRP) hybrid composites tested with 30 J impact energy was the seawater degradation environment (Fig. 21). It was calculated that the maximum contact force value of the composites at room temperature decreased by 35.096% in GFRP composites, 46.099% in CFRP composites and 35.797% in GCFRP composites after 90 days of aging in seawater.

When looking at the effects of aging environment; at 30 Joule impact energy, the impact strength of GFRP and GCFRP composites decreased and the transition from penetration to perforation began, and it was determined that penetration to full perforation was more evident in CFRP composites (Fig. 22). In GFRP and GCFRP composites, the maximum deflection increased as they approached perforation, that is, full perforation, due to the effect of the seawater aging environment. Maximum deflection values of GFRP and GCFRP composites at room temperature; it was calculated that GFRP composites increased by 39.506% and GCFRP composites increased by 41.08% by aging in a seawater environment for 90 days. CFRP composites, which achieved full perforation at 30 Joule impact energy under room temperature conditions, showed perforations at lower contact forces due to aging, thus their collapse values decreased. It was calculated that it decreased by 21.211% compared to the deflection values in the normal environment due to 90 days of seawater aging (Fig. 22). It has been concluded that the environments that have the most reducing effect on the impact strength of composites subjected to low-velocity impact testing under aging environmental conditions and durations are seawater environment

and machine oil environment. It has been determined that the impact resistance of the diesel fuel aging medium is higher than the other two aging environments. Damage images of composites subjected to low-velocity impact testing at 30 joules impact energy are shown in Fig. 23. It is understood the level of puncture damage on the front and back surfaces of the composites that have been impacted.

3.5. Morphological analysis

It was aimed to examine the changes in the morphological structure of the broken composite parts within the material after the tensile test samples of glass/epoxy (GFRP), carbon/epoxy (CFRP) and glass-carbon/epoxy (GCFRP) hybrid composites produced with VARTM. Morphological analyzes of composite samples were performed on a Leo Evo 40 scanning electron microscope (SEM) device with a capacity of 20 kV. Since the aging environment that most affects the strength of composites is the artificial 90-day aged seawater environment, changes in the internal structure of the material were examined by taking images from a scanning electron microscope (SEM) in order to determine the morphological analysis. SEM analyzes of samples damaged as a result of tensile tests of composites at room temperature and composites kept in seawater for 90 days were compared. The SEM analysis of GFRP composites, where the morphological analysis of the broken parts after the tensile test at room temperature is performed, is shown in Fig. 24, the SEM analysis of CFRP composites is shown in Fig. 25, and the SEM analysis of GCFRP hybrid composites is shown in Fig. 26.

When zoomed in on the glass fiber, the images of the broken fibers are shown in detail. It is clearly shown that there appears to be very little matrix phase around the broken fibers. This analysis reveals that damage occurs in areas where fiber-matrix interface adhesion is weak (Fig. 24).

Morphological analyzes of carbon/epoxy (CFRP) composites under normal environmental conditions were evaluated at different micron sizes. By getting closer to the carbon fiber, the appearance of the carbon fiber structure and the epoxy matrix element after damage is shown in detail. It has been determined that interlayer separation and delamination occur in areas where the matrix element is shallow. When approaching the damage area where the carbon fibers broke, air gaps in the epoxy matrix were detected (Fig. 25). By getting closer to the GCFRP hybrid composites after damage, the appearance of reinforcement of glass-carbon fiber layers with epoxy matrix element is shown in detail. It has been observed that delamination damage, where the glass and carbon layers separate from each other, occurs in areas where the matrix element is shallow. When approaching the damage area where carbon-glass fibers are broken, slight agglomerations of epoxy matrices can be seen on the broken fibers (Fig. 26).

The SEM analysis of GFRP, CFRP and GCFRP composites, where the morphological analysis of the broken parts after the tensile test of the composites aged for 90 days in seawater is shown in Fig. 27. Morphological analyzes of GFRP, CFRP and GCFRP composites aged in seawater for 90 days were evaluated at lower micron sizes compared to composite samples at room temperature conditions.

Agglomerations of epoxy matrixes accumulated on the broken glass fibers. It has been determined that the glass layers are separated more clearly due to the aging effect (Fig. 27 (a)). In Fig. 27 (b), agglomerations of epoxy matrices accumulated on the broken carbon fibers.

It can be interpreted as a weakening of mechanical properties due to the decrease in adhesion between reinforcement-matrix phases due to the effect of seawater. In this case, it is interpreted that the fibers are broken and separated from each other by delamination, where the carbon layers are separated more clearly due to the aging effect. The adhesion strength of the epoxy matrix at the interface of the glass-carbon hybrid layers shown in Fig. 27 (c) was examined closely. Adhesion force, which is an important mechanical condition in the strength of the adhesion between epoxy-fiber, decreased with the effect of seawater aging, making fiber breaks and separations more obvious.

4. Conclusion

In all aging environments; It was concluded that the average absorption percentage value of GCFRP composites was higher than that of GFRP composites and less than the absorption percentage value of CFRP composites. It was calculated that the difference between the mass absorption percentage values in all composite samples occurred between 30 days (720 hours) and 60 days (1440 hours). When the effect of environments on absorption values is examined; It was concluded that the highest absorption values were in the machine oil environment and the lowest absorption values were in the diesel fuel environment.

When looking at the tensile test behaviors of the aging environment effects of GFRP, CFRP and GCFRP composites, it was concluded that the environment that affects the mechanical strength the most is the seawater environment, while the environment that affects the least is the diesel fuel environment. It was concluded that the elasticity modulus of GFRP composites in normal room conditions after aging in seawater for 90 days decreased by 17.01%, the elasticity modulus of CFRP composites decreased by 16.37% and the elasticity modulus of GCFRP composites decreased by 10.42%.

When the three-point bending test behaviors of GFRP, CFRP and GCFRP composites' aging environment effects are examined, it is concluded that the environment that affects the mechanical strength the most is the seawater environment, while the environment that affects the mechanical strength the least is the diesel fuel environment. The tensile strength of the composites at room temperature with the effect of 90-day seawater aging; It was concluded that it reduced the bending tensile strength by 18.37% in GFRP composites, 26.18% in CFRP composites, and 17.46% in GCFRP composites.

The glass-carbon hybridization effect has a very low effect on bending strength, causing it to be the composite type with the least strength under aging effect.

As a result of the low- velocity impact behavior of GFRP, CFRP and GCFRP composites, it was concluded that the most durable composite type is glass/epoxy (GFRP) composites. The reason why glass/epoxy composites are more durable than carbon/epoxy (CFRP) composites is that glass fibers are more ductile

against impact load. Carbon fibers, on the other hand, are more brittle than glass fibers. It was concluded that the impact resistance of GCFRP hybrid composites formed by aligning the upper and lower layers with glass fibers, with carbon fibers in the center, increased. It was concluded that the hybridization effect increases the low- velocity impact strength under all aging environment conditions.

It has been concluded that the aging environment that most affects the low- velocity impact strength of GFRP, CFRP and GCFRP composites is seawater, engine oil and diesel fuel, in order from highest to lowest. It was concluded that the maximum contact force value of the composites at room temperature decreased by 35.096% in GFRP composites, 35.933% in CFRP composites, and 35.797% in GCFRP hybrid composites due to the 90-day seawater aging effect.

In the morphological analysis of GFRP, CFRP and GCFRP composites after tensile test damage; It was concluded that delamination and fiber cracks were damaged at the fracture point, where the presence of the epoxy matrix decreased. It was concluded that the hybridization effect is a solid combination and increases the strength. It was estimated that the damage started at lower loads because matrix degradation occurred under the influence of seawater.

Suggestions for the study and general evaluation; Choosing a woven fabric of glass and carbon fibers is a situation that affects mechanical strength. It is thought that choosing glass and carbon fibers with different fiber orientations will affect mechanical strength. In this regard; Composites with different sequences can be produced to increase the glass-carbon hybridization effect. For the seawater environment that affects the aging effect the most, polymer matrices that are stronger against corrosion may be preferred. It was concluded that all of the composite types tested in the study had very good durability regarding their mechanical and tribological behavior in the engine oil environment and petroleum oil environment. These results are on the brink; lass/epoxy, carbon/epoxy and glass-carbon/hybrid composites can be considered to be preferred over traditional metal structures in the durability preference of oil tanks, oil tanks or machine elements where such environments are used.

Declarations

Acknowledgements

The author(s) announced the following financial support for the research of this article: This study was supported by the Scientific Research Projects Coordination Unit of Inonu University (Project ID: 1822).

Author information

Authors and Affiliations

Faculty of Engineering and Architecture, Department of Mechanical Engineering, Faculty of University of Mus Alparslan University, Mus, 4250, Turkey, Ahmet Saylık.

Faculty of Engineering, Department of Mechanical Engineering, Inonu University, Malatya, 44280, Turkey, Şemsettin Temiz.

Contributions

AS conceived the study, main conceptual ideas, and prepared the original manuscript. AS produced the plates for all composite materials to be prepared for the experimental study. AS performed tensile, three-point bending test and low-velocity impact tests in the experimental study. ŞT helped interpret the data analyzed as a result of the tests and edit the article.

Corresponding author

Correspondence to Ahmet Saylık.

Ethics declarations

Conflict of interest

The authors declare no conflicts of interest.

Data and code availability

Not Applicable.

Supplementary information

Not Applicable.

Ethical approval

The authors clearly declare that this study is an ethical study.

References

1. Felipe RCTS, Felipe RNB, Batista ACMC, Aquino EMF (2019) Influence of environmental aging in two polymer-reinforced composites using different hybridization methods: Glass/Kevlar fiber hybrid strands and in the weft and warp alternating Kevlar and glass fiber strands. Compos Part B: Eng 174:106994. https://doi.org/10.1016/j.compositesb.2019.106994
2. Nakada M, Miyano Y, Kinoshita M, Koga MR, Okuya T (2002) Time-temperature dependence of tensile strength of unidirectional CFRP. J Compos Mater 36:2567–2581. https://doi.org/10.1106/002199802027292
3. Kumar BG, Singh RP, Nakamura T (2002) Degradation of carbon fiber-reinforced epoxy composites by ultraviolet radiation and condensation. J Compos Mater 36:2713–2733. https://doi.org/10.1177/002199802761675511

4. Shin KB, Kim CG, Hong CS (2003) Correlation of accelerated aging test to natural aging test on graphite-epoxy composite materials. J Reinf Plast Compos 22:849–861. https://doi.org/10.1177/0731684403022009005
5. Peterson EC, Patil RR, Kallmeyer AR, Kellogg KG (2008) A micromechanical damage model for carbon fiber composites at reduced temperatures. J Compos Mater 42:2063–2082. https://doi.org/10.1177/0021998308094547
6. Shokrieh MM, Bayat A (2007) Effects of ultraviolet radiation on mechanical properties of glass/polyester composites. J Compos Mater 41:2443–2455. https://doi.org/10.1177/0021998307075
7. Sharma SC, Bayat A (2006) Studies on the weathering behavior of glass coir polypropylene composites. J Reinf Plast Compos 25:925–932. https://doi.org/10.1177/073168440606355
8. Mahato KK, Shukla MTJ, Kumar DS, Ray BC (2014) In service performance of fiber reinforced polymer composite in different environmental conditions: A Review. J Adv Res Manuf Mater Sci Metall Eng 1:55–88
9. Velmurugan G, Shaafi T, Bhagavathi MS, Siva SV (2022) Evaluate the tensile, flexural and impact strength of hemp and flax based hybrid composites under cryogenic environment, Materials Today: Proceedings 50 1326–1332. https://doi.org/10.1016/j.matpr.2021.08.244
10. Zeltmann SE, Poveda RL, Gupta N (2015) Accelerated environmental degradation and residual flexural analysis of carbon nanofiber reinforced composites. Polym Degrad Stab 121:348–358. https://doi.org/10.1016/j.compositesa.2019.105718
11. Chiang CL, Chou HY, Shen MY (2020) Effect of environmental aging on mechanical properties of graphene nanoplate-let/nanocarbon aerogel hybrid-reinforced epoxy/carbon fiber composite laminates. Compos Part A: Appl Sci Manufac 130:105718. http://dx.doi.org/10.1016/j.polymdegradstab.2015.09.022
12. Nayak BA, Prusty RK, Ray BC (2020) Effect of nanosilica and nanoclay reinforcement on flexural and thermal properties of glass fiber/epoxy composites, Materials Today: Proceedings 33 5098–5102. https://doi.org/10.1016/j.matpr.2020.02.852
13. Kootsookos A, Mouritz AP (2004) Seawater durability of glass- and carbon-polymer composites. Compos Sci Technol 64:1503–1511. https://doi.org/10.1016/j.compscitech.2003.10.019
14. Mula S, Bera T, Ray PK (2005) Effects of hydrothermal aging on mechanical behavior of subzero weathered GFRP composites. J Reinf Plast Compos 25:673–680. https://doi.org/10.1177/073168440606024
15. Aldajah S, Alawsi G, Rahmaan SA (2009) Impact of sea and tap water exposure on the durability of GFRP laminates. Mater Design 30:1835–1840. https://doi.org/10.1016/j.matdes.2008.07.044
16. Trujillo EJ, González CR, González JAR (2018) Seawater ageing effect on the mechanical properties of composites with different fiber and matrix types. J Compos Mater 0:1–13. https://doi.org/10.1177/0021998318811514

17. Bonsu AO, Liang W, Mensah C, Yang B (2022) Assessing the mechanical behavior of glass and basalt reinforced vinyl ester composite under artificial seawater environment. Structures 38:961–978. https://doi.org/10.1016/j.istruc.2022.02.053
18. Sebaey TA (2022) Crashworthiness of GFRP composite tubes after aggressive environ-mental aging in seawater and soil. Compos Struct 284:115105. https://doi.org/10.1016/j.compstruct.2021.115105
19. Cheng M, Zhong Y, Kureemun U, Cao D, Hu H, Lee HP, Li S (2020) Environmental durability of carbon/flax fiber hybrid composites. Compos Struct 234:111719. https://doi.org/10.1016/j.compstruct.2019.111719
20. Humeau C, Davies P, Jacquemin F (2018) An experimental study of water diffusion in carbon/epoxy composites under static tensile stress. Compos Part A: Appl Sci Manufac 107:94–104. https://doi.org/10.1016/j.compositesa.2017.12.016
21. Dlouhy I, Chlup Z, Boccaccini DN, Atiq S, Boccaccini AR (2003) Fracture behaviour of hybrid glass matrix composites: Thermal ageing effects. Compos Part A: Appl Sci Manufac 34(12):1177–1185. https://doi.org/10.1016/j.compositesa.2003.08.004
22. Tsai YI, Bosze EJ, Barjasteh E, Nutt SR (2009) Influence of hygrothermal environment on thermal and mechanical properties of carbon fiber/fiberglass hybrid composites. Compos Sci Technol 69:432–437. https://doi.org/10.1016/j.compscitech.2008.11.012
23. Firdosh S, Tamrakar S, Firdosh S, Murth HNN, Pal R, Angadi G, Raghavendra N, Krishna M (2015) Durability of GFRP nanocomposites subjected to hygrothermal ageing. Compos Part B: Eng 69:443–451. http://dx.doi.org/10.1016/j.compositesb.2014.09.028
24. Tamrakar S, Kiziltas A, Mielewski D, Zander R (2021) Characterization of kenaf and glass fiber reinforced hybrid composites for underbody shield applications. Compos Part B: Eng 216:108805. https://doi.org/10.1016/j.compositesb.2021.108805
25. Atas C, Dogan A (2015) An experimental investigation on the repeated impact response of glass/epoxy composites subjected to thermal ageing. Compos Part B: Eng 75:127–134. http://dx.doi.org/10.1016/j.compositesb.2015.01.032
26. Lobanov DS, Zubova EM (2020) Temperature aging effects on mechanical behavior of structural GFRP on interlaminar shear tests, IOP Conference Series: Materials Science and Engineering 747 012119. https://doi.org/10.1088/1757-899X/747/1/012119
27. Mansouri L, Djebbar A, Khatir S, Wahab M (2019) Effect of hygrothermal aging in distilled and saline water on the mechanical behaviour of mixed short fiber/woven composites. Compos Struct 207:816–825. https://doi.org/10.1016/j.compstruct.2018.09.067
28. Zai BA, Park MK, Choi HS, Mehboob H (2009) Effect of moisture absorption on damping and dynamic stiffness of carbon fiber/epoxy composites. J Mech Sci Technol 23:2998–3004. https://doi.org/10.1007/s12206-009-0908-0
29. Tanks JD, Arao Y, Kubouchi M (2018) Diffusion kinetics, swelling, and degradation of corrosion-resistant C-glass/epoxy woven composites in harsh environments. Compos Struct 202:686–694.

https://doi.org/10.1016/j.compstruct.2018.03.078

30. Li C, Xian G, Li H (2018) Influence of immersion in water under hydraulic pressure on the interfacial shear strength of a unidirectional carbon/glass hybrid rod. Polym Test 72:164–171. https://doi.org/10.1016/j.polymertesting.2018.10.004
31. Li C, Yin X, Liu Y, Guo R, Xian G (2020) Long-term service evaluation of a pultruded carbon/glass hybrid rod exposed to elevated temperature, hydraulic pressure and fatigue load coupling. Int J Fatigue 134:105480. https://doi.org/10.1016/j.ijfatigue.2020.105480
32. Li C, Li C, Yin X, Wang Y, Zhang L, Zhang Z, Liu Y, Xian G (2020) Mechanical property evolution and service life prediction of pultruded carbon/glass hybrid rod exposed in harsh oil-well condition. Compos Struct 246:112418. https://doi.org/10.1016/j.compstruct.2020.112418
33. Rathore DK, Prusty RK, Mohanty SC, Singh BP, Ray BC (2017) In-situ elevated temperature, flexural and creep response of inter-ply glass/carbon hybrid FRP composites. Mech Mater 105:99–111. http://dx.doi.org/10.1016/j.mechmat.2016.11.013
34. Ghabezi P, Harrison N (2020) Mechanical behavior and long-term life prediction of carbon/epoxy and glass/epoxy composite laminates under artificial seawater environment. Mater Lett 261:127091. https://doi.org/10.1016/j.matlet.2019.127091
35. Chen D, Suna G, Meng M, Jin X, Li Q (2019) Flexural performance and cost efficiency of carbon/basalt/glass hybrid FRP composite laminates. Thin-Walled Struct 142:516–531. https://doi.org/10.1016/j.tws.2019.03.056
36. Kaybal HB, Ulus H, Eskizeybek V, Avcı A (2021) An experimental study on low velocity impact performance of bolted composite joints-part 2: Influence of long-term seawater aging. Compos Struct 272:113571. https://doi.org/10.1016/j.compstruct.2021.113571
37. Saylık A, Temiz Ş (2022) Low-speed impact behavior of fiber-reinforced polymer-based glass, carbon, and glass/carbon hybrid composites. Mater Test 64:820–831. https://doi.org/10.1515/mt-2021-2179
38. Rajan BG, Padmanabhan S, Lakshmi Ganesh R, Mani Chandana K, Lavanya E (2021) Low velocity impact analysis of carbon/glass/epoxy hybrid composite pipes, Materials Today: Proceedings 47 4181–4188. https://doi.org/10.1016/j.matpr.2021.04.454
39. Satkar AR, Mache A, Kulkarni A (2022) Numerical investigation on perforation resistance of glass-carbon/epoxy hybrid composite laminate under ballistic impact, Materials Today: Proceedings 59 734–741. https://doi.org/10.1016/j.matpr.2021.12.464
40. Xian G, Guo R, Li C, Hong B (2023) Mechanical properties of carbon/glass fiber reinforced polymer plates with sandwich structure exposed to freezing-thawing environment: Effects of water immersion, bending loading and fiber hybrid mode. Mech Adv Mater Struct 30:814–834. https://doi.org/10.1080/15376494.2021.2024927
41. Papa I, Ricciardi MR, Calzolari A, Langella A, Tirillò J, Sarasini F, Lopresto V (2021) Mechanical behavior and damage degree of hybrid glass/carbon composites at low temperature. Polym Compos 42:2432–2444. https://doi.org/10.1002/pc.25989

42. Ghabezi P, Harrison NM (2022) Hygrothermal deterioration in carbon/epoxy and glass/epoxy composite laminates aged in marine-based environment (degradation mechanism, mechanical and physicochemical properties). J Mater Sci 57:4239–4254. https://doi.org/10.1007/s10853-022-06917-2
43. Guo R, Xian G, Li F, Li C, Hong B (2022) Hygrothermal resistance of pultruded carbon, glass and carbon/glass hybrid fiber reinforced epoxy composites. Constr Build Mater 315:125710. https://doi.org/10.1016/j.conbuildmat.2021.125710
44. Jesthi DK, Saroj S, Nayak S (2022) The influence of seawater on mechanical properties of hybrid carbon and glass fiber polymer composites, Materials Today: Proceedings 49 507–509. https://doi.org/10.1016/j.matpr.2021.03.210
45. Jesthi DK, Nayak S (2019) Evaluation of mechanical properties and morphology of seawater aged carbon and glass fiber reinforced polymer hybrid composites. Compos Part B 174:106980. https://doi.org/10.1016/j.compositesb.2019.106980
46. Xian G, Guo R, Li C (2022) Combined effects of sustained bending loading, water immersion and fiber hybrid mode on the mechanical properties of carbon/glass fiber reinforced polymer composite. Compos Struct 281:115060. https://doi.org/10.1016/j.compstruct.2021.115060
47. Pan Y, Yan D (2021) Study on the durability of GFRP bars and carbon/glass hybrid fiber reinforced polymer (HFRP) bars aged in alkaline solution. Compos Struct 261:113285. https://doi.org/10.1016/j.compstruct.2020.113285
48. Amaro AM, Reis PNB, Neto MA, Louro C (2014) Effect of different commercial oils on mechanical properties of composite materials. Compos Struct 118:1–8. http://dx.doi.org/10.1016/j.compstruct.2014.07.017
49. Hussnain SM, Shah SZH, Megat-Yusoff PSM, Hussain MZ (2023) Degradation and mechanical performance of fibre-reinforced polymer composites under marine environments: A review of recent advancements. Polym Degrad Stab 215:110452. https://doi.org/10.1016/j.polymdegradstab.2023.110452
50. ASTM D570-98, Standard Test Method for Water Absorption of Plastics, ASTM International: West Conshohocken (2018)
51. ASTM D3039/D3039M-08 (2008) Standard Test Method for Tensile Properties of Polymer Matrix Composite Materials. ASTM International, Singapore
52. ASTM Standard D7264 (2007) Standard Test Method for Flexural Properties of Polymer Matrix Composite Materials. ASTM International, West Conshohocken PA
53. ASTM D7136/D7136M-15, Standard Test Method for Measuring the Damage Resistance of a Fiber-Reinforced Polymer Matrix Composite to a Drop-Weight Impact Event, West Conshohocken, Pennsylvania, USA, ASTM International (2015)

Figures

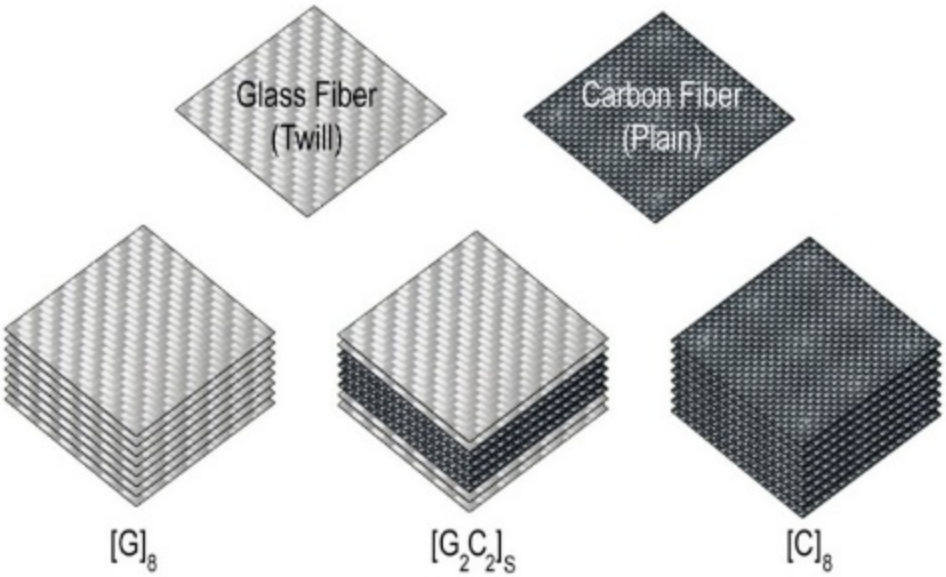

Figure 1

Laminate codes and labeling system of stacking order.

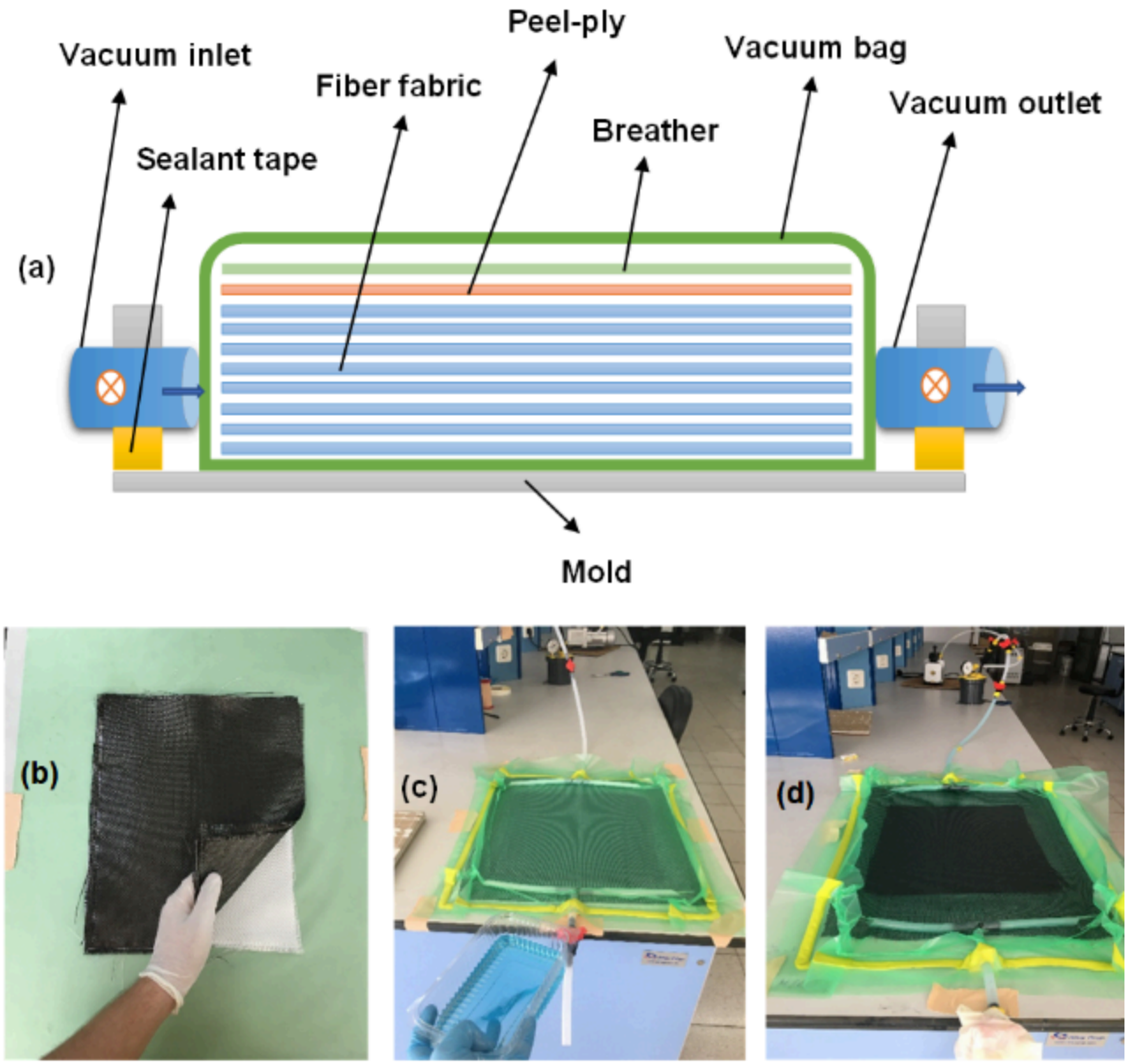

Figure 2

Preparation of composites: (a) VARTM scheme, (b) stacking of fibers, (c) transferring the resin to the vacuum environment, (d) vacuum environment.

Figure 3

The process of placing composites into degradation environments.

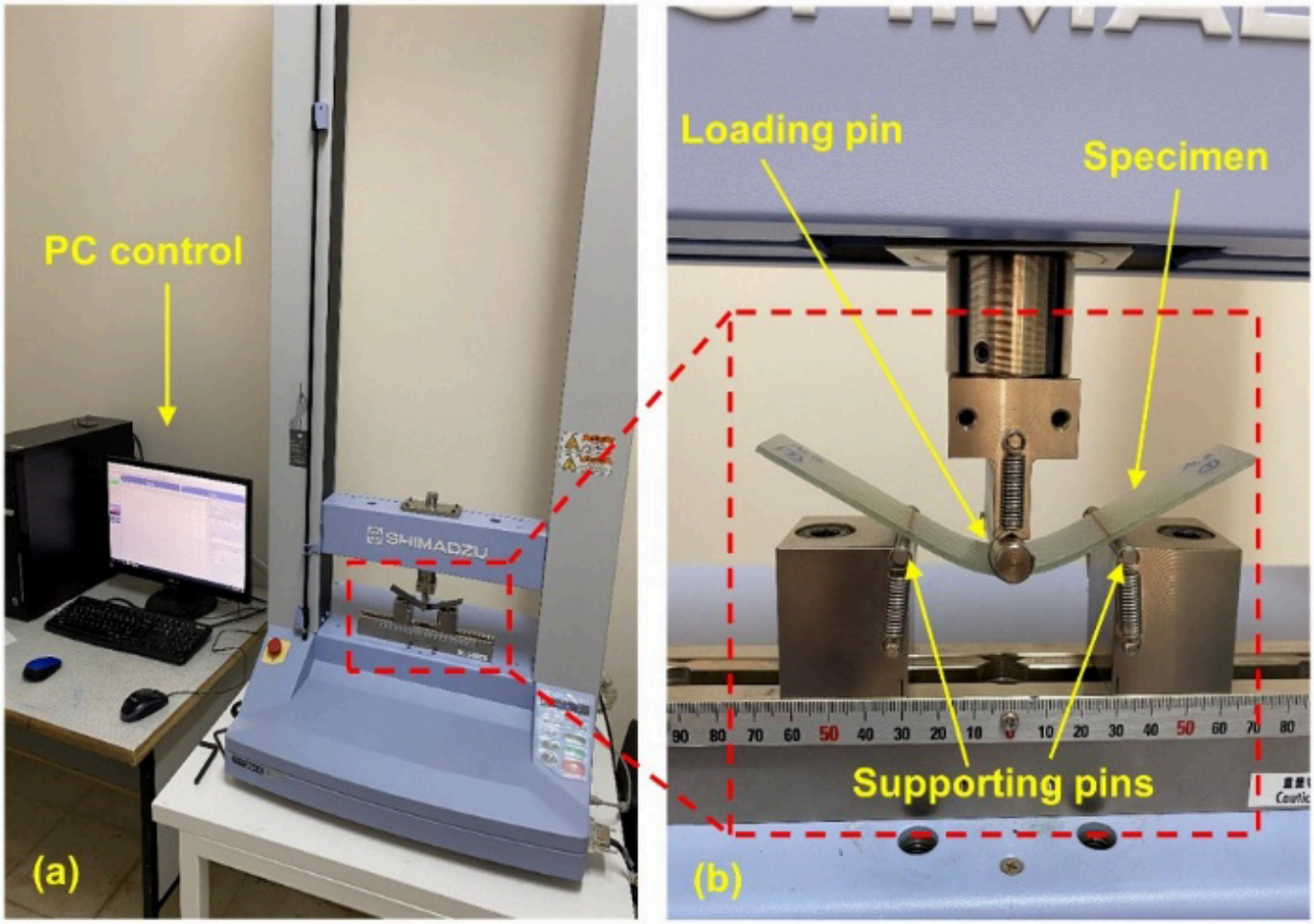

Figure 4

Bending test setup: (a) Shimadzu AGS-X tester, (b) there-point bending test.

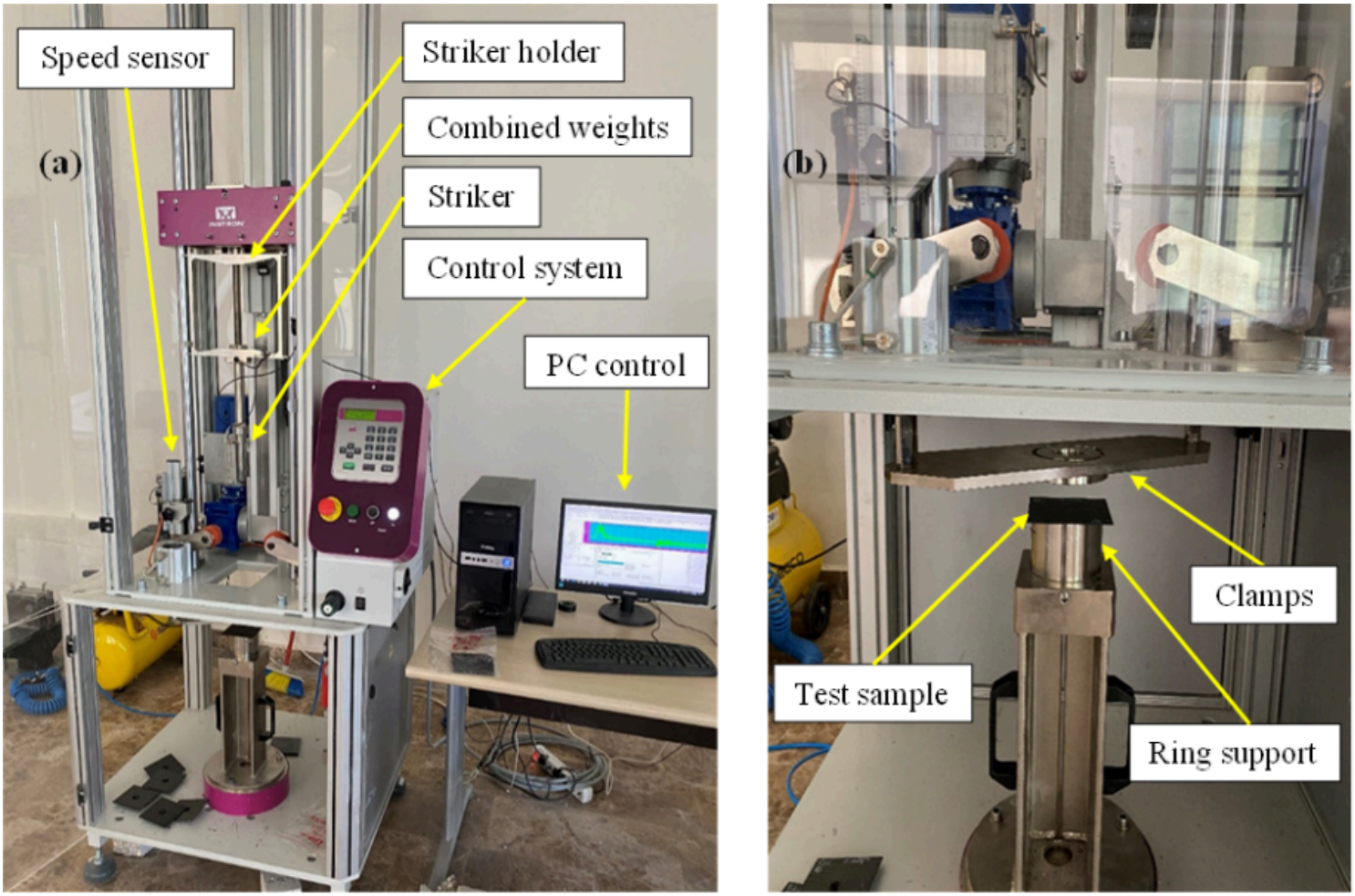

Figure 5

INSTRON CEAST 9350 impact tester; **(a)** device system, and **(b)** test chamber.

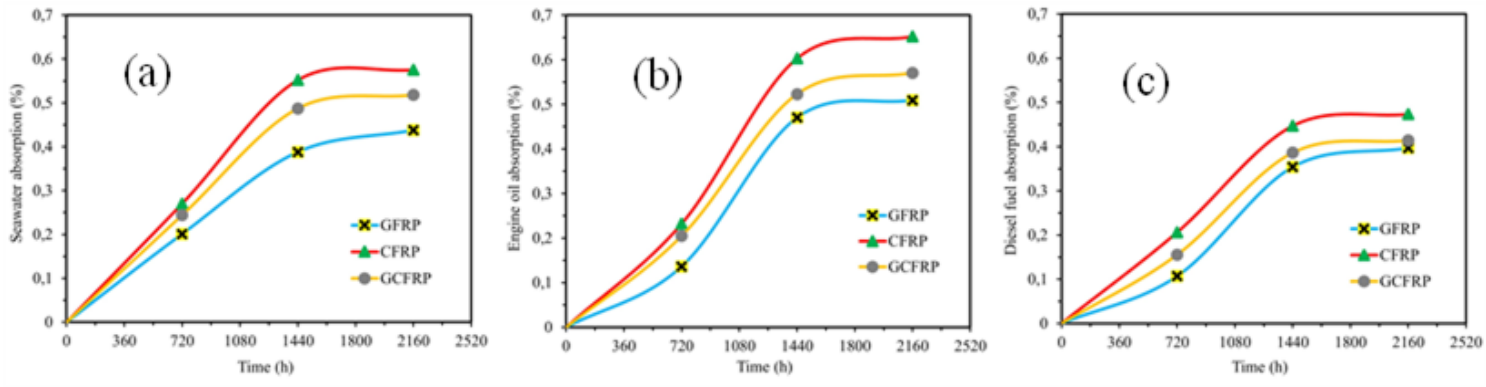

Figure 6

Absorption weight percent change of aged GFRP, CFRP and GCFRP composite samples: (a) seawater, (b) engine oil, (c) diesel fuel.

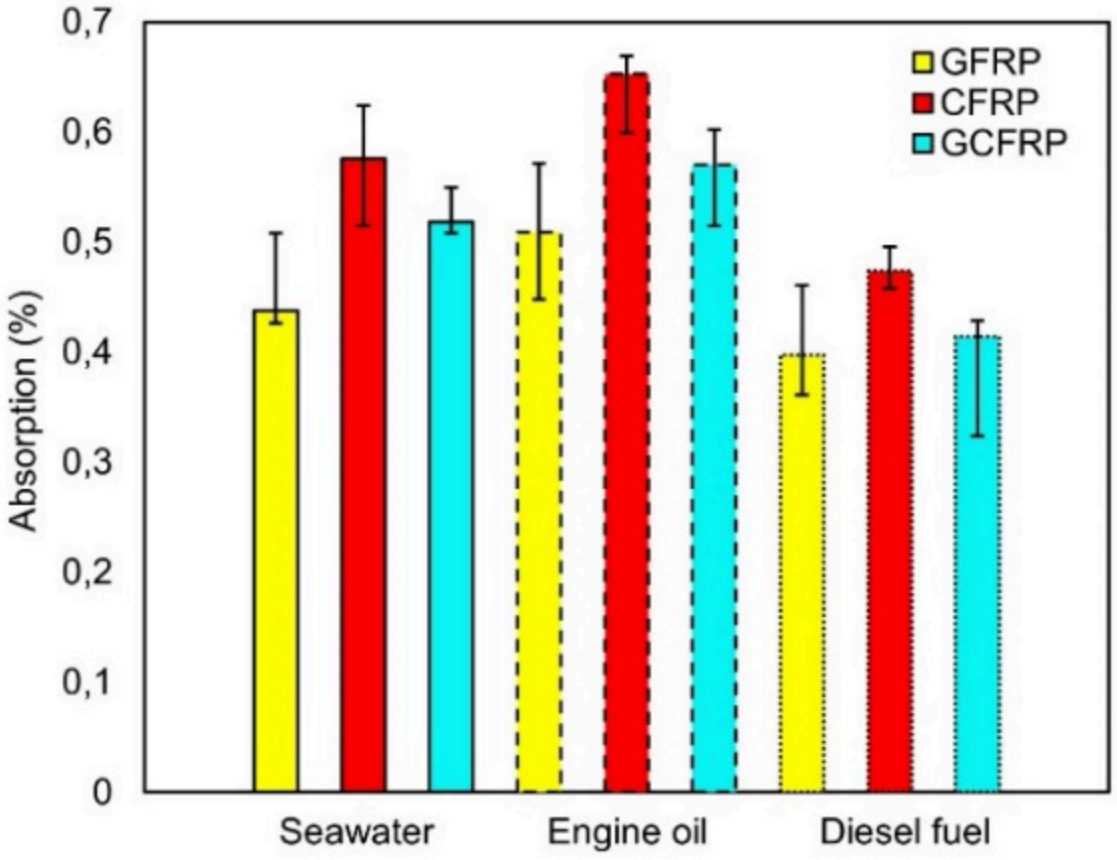

Figure 7

The mean percentage change in absorption of CFRP, GFRP and GCFRP composite specimens aged for 90 days in artificial seawater, engine oil and diesel fuel environments.

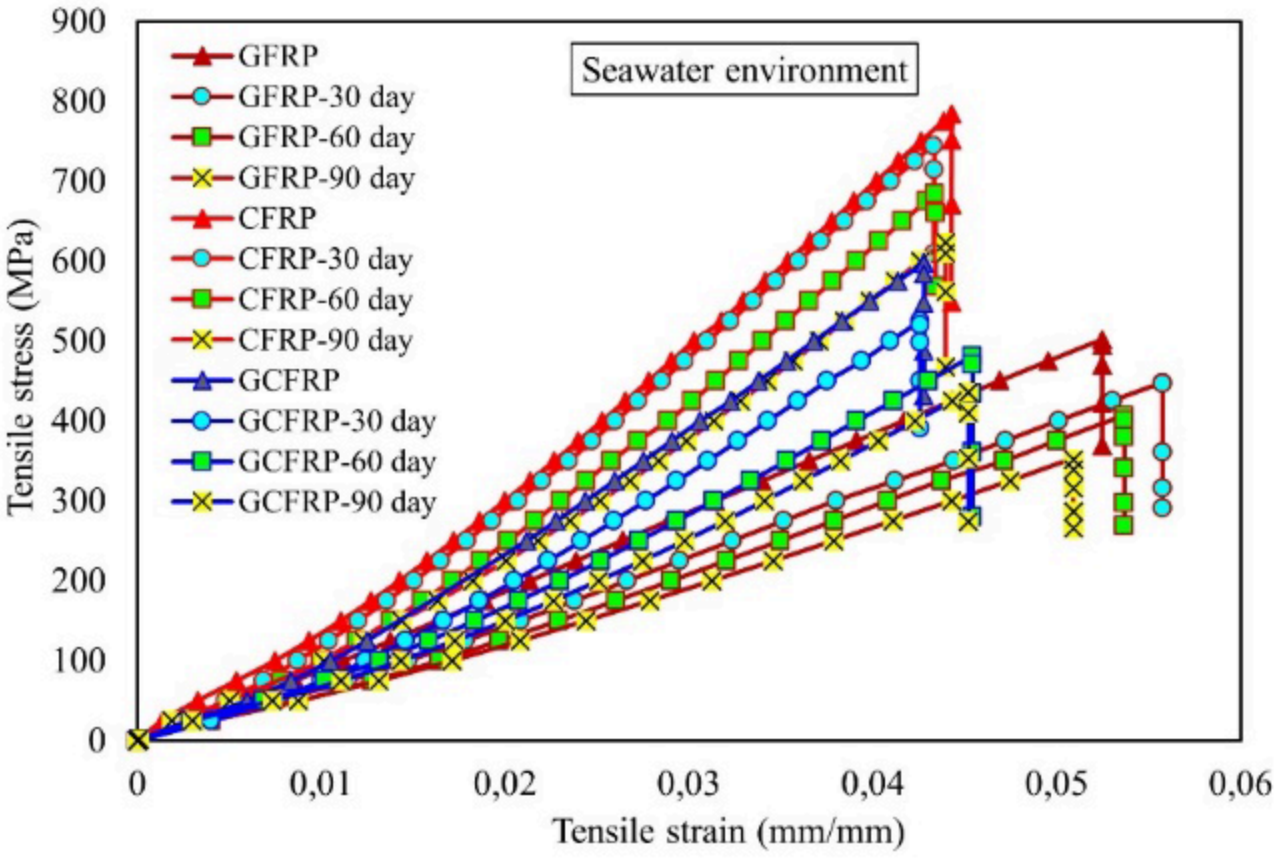

Figure 8

Stress-strain of GFRP, CFRP and GCFRP composites aged in seawater environment.

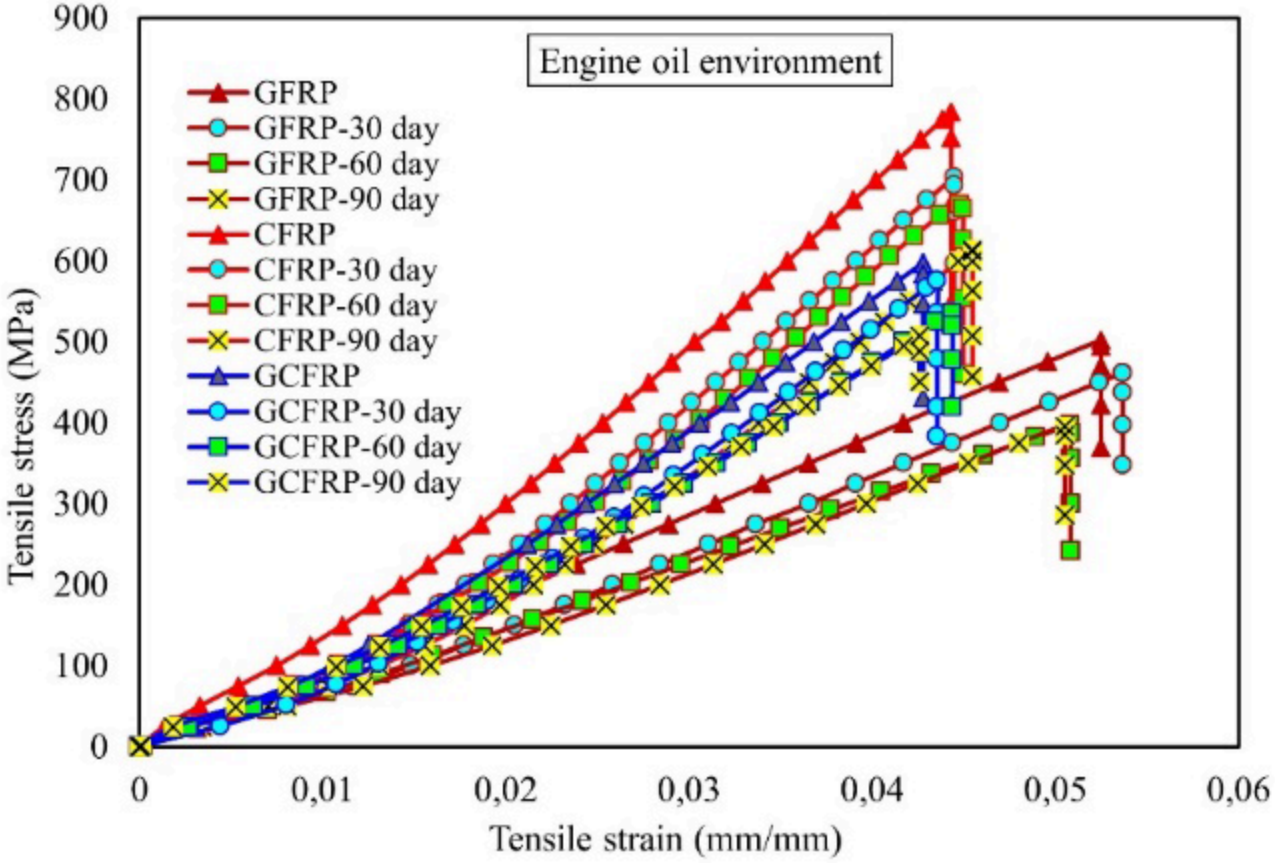

Figure 9

Stress-strain of GFRP, CFRP and GCFRP composites aged in engine oil environment.

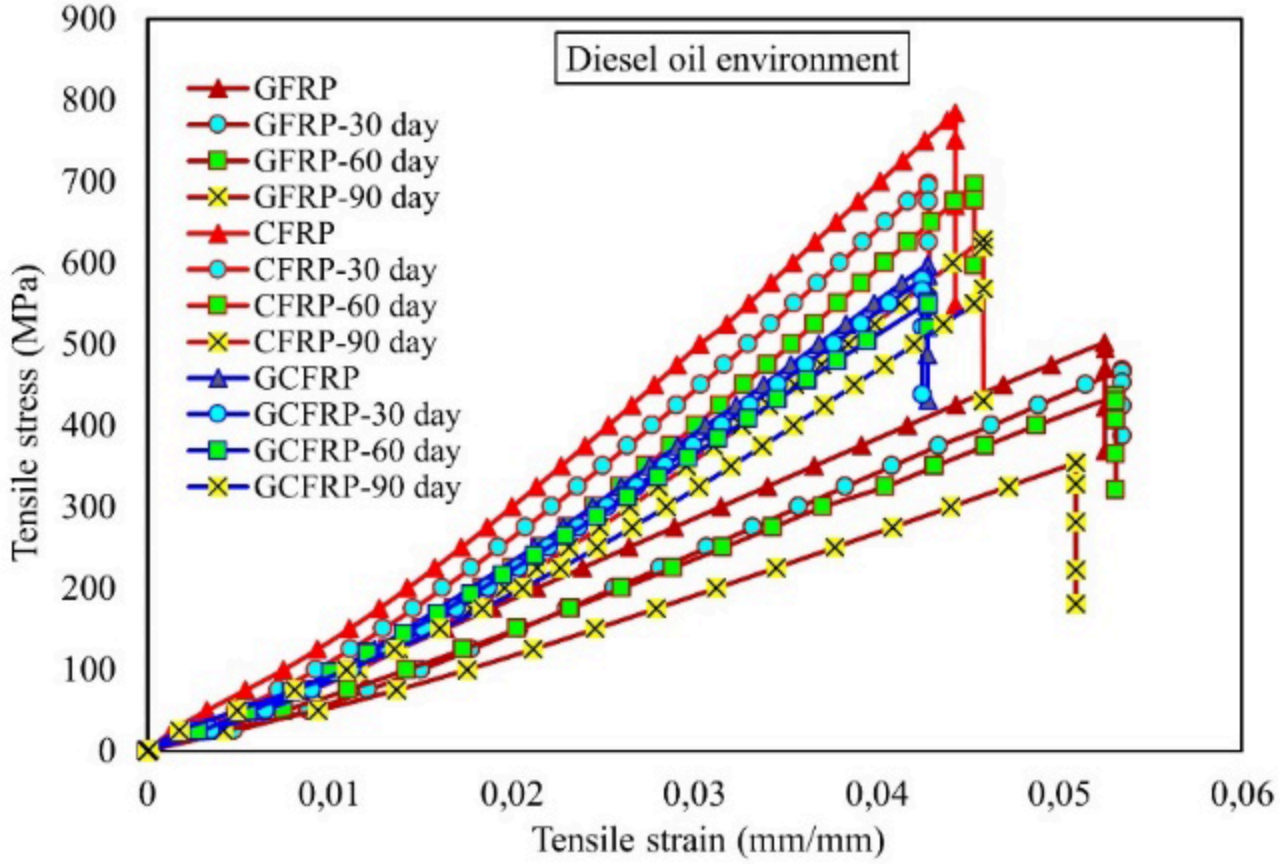

Figure 10

Stress-strain of GFRP, CFRP and GCFRP composites aged in diesel oil environment.

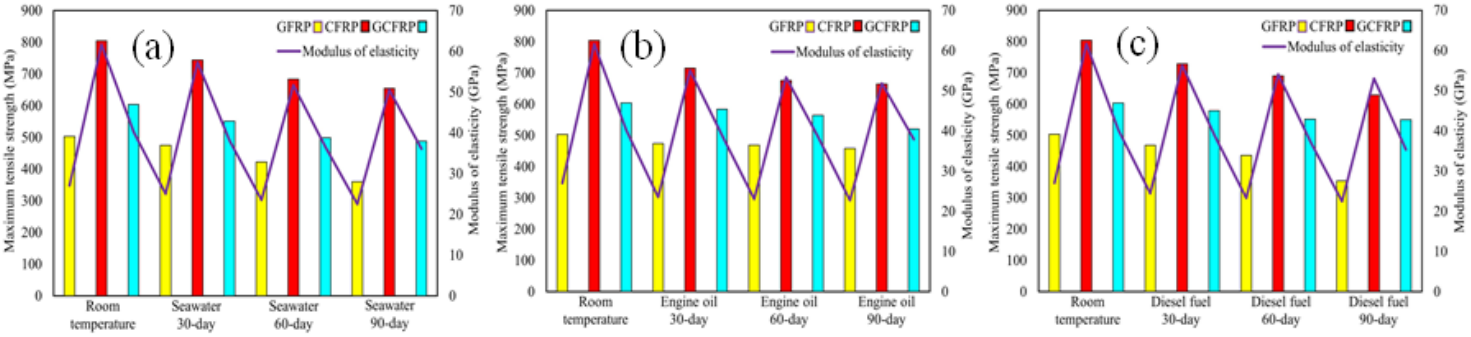

Figure 11

Comparison of maximum tensile stress and modulus of elasticity of GFRP, CFRP and GFRP composites aged; (a) seawater, (b) engine oil, (c) diesel fuel.

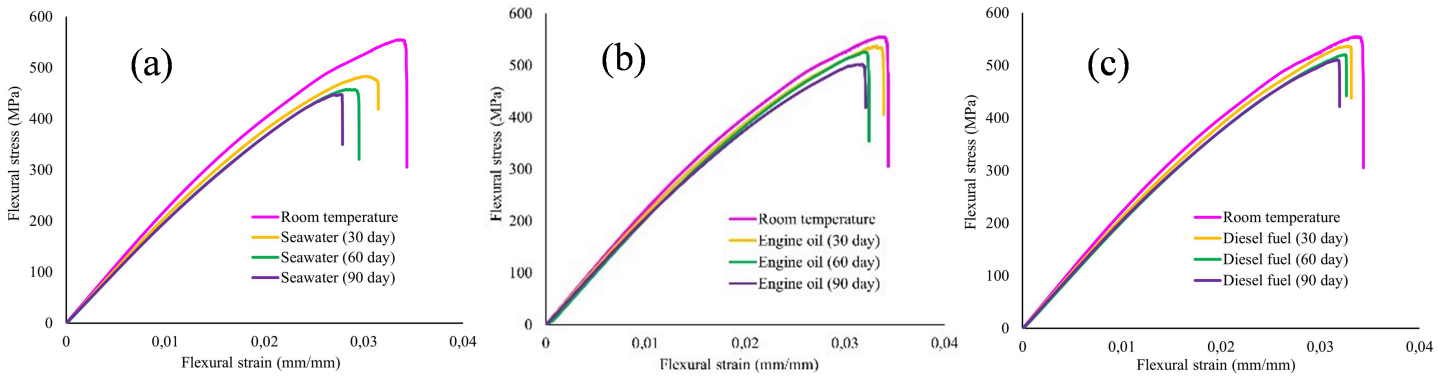

Figure 12

Flexural stress-strain comparison of GFRP composites according to aging environments for 30, 60 and 90 days; (a) seawater, (b) engine oil, (c) diesel fuel.

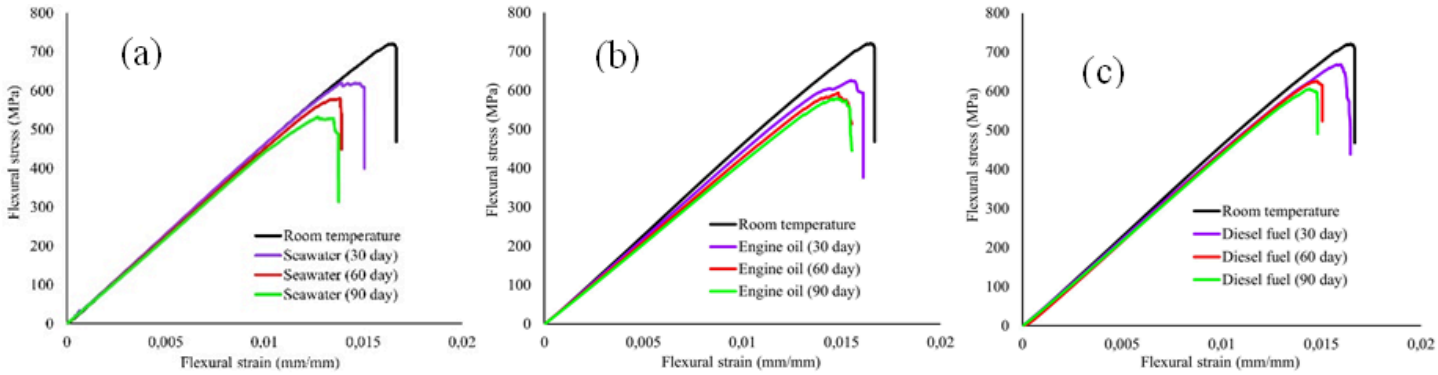

Figure 13

Flexural stress-strain comparison of CFRP composites according to aging environments for 30, 60 and 90 days; a) seawater, b) engine oil c) diesel fuel.

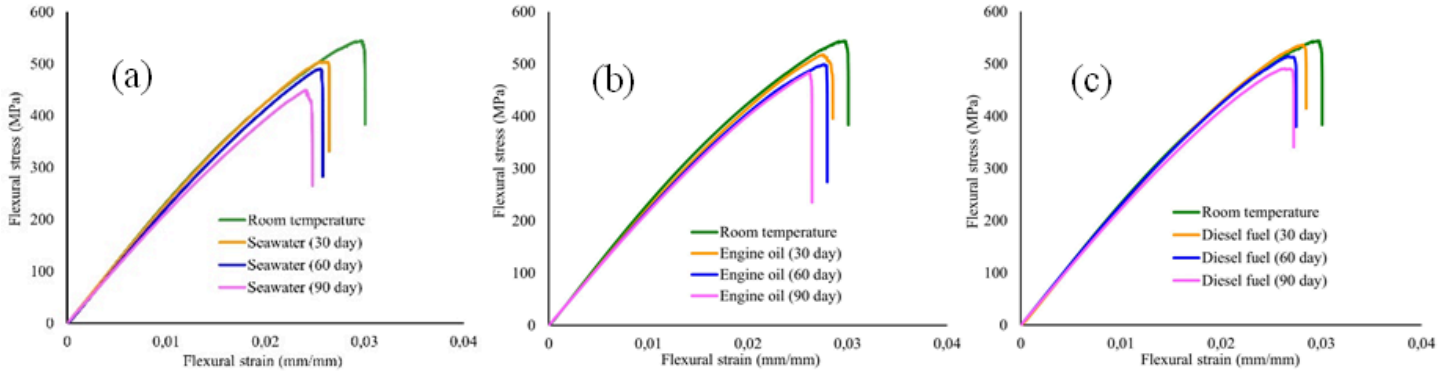

Figure 14

Flexural stress-strain comparison of GCFRP composites according to aging environments for 30, 60 and 90 days; (a) seawater, (b) engine oil, (c) diesel fuel.

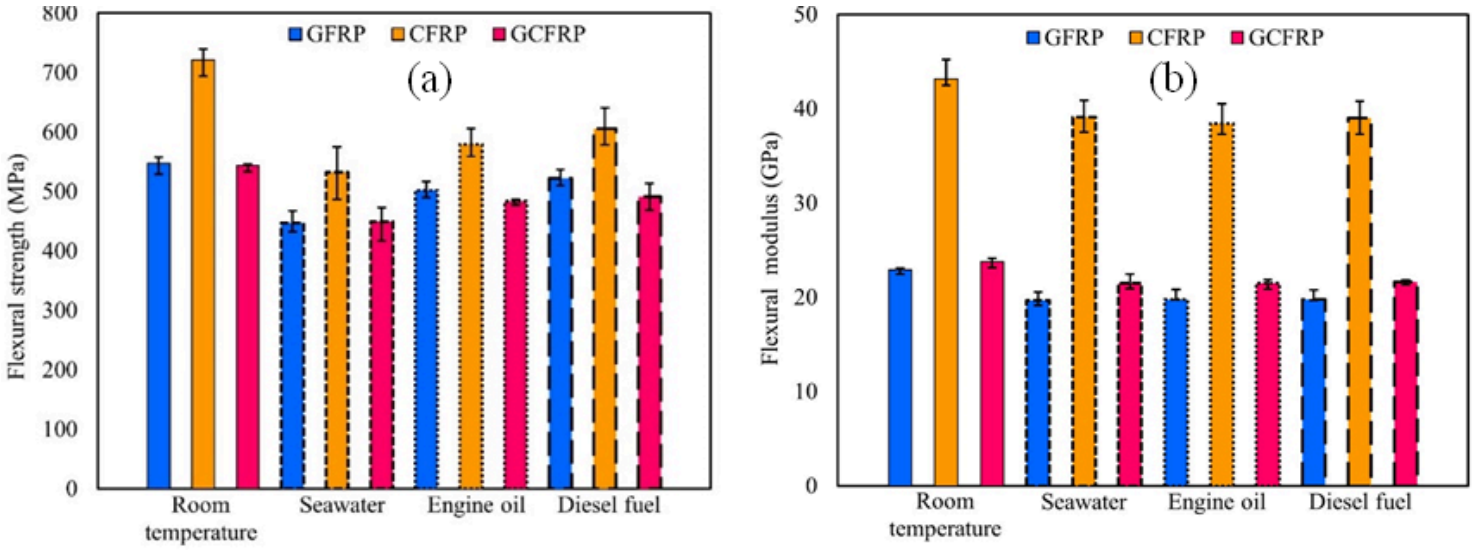

Figure 15

Comparison of the mean flexural strengths and flexural modulus of CFRP, GFRP and GCFRP composites aged for 90 days.

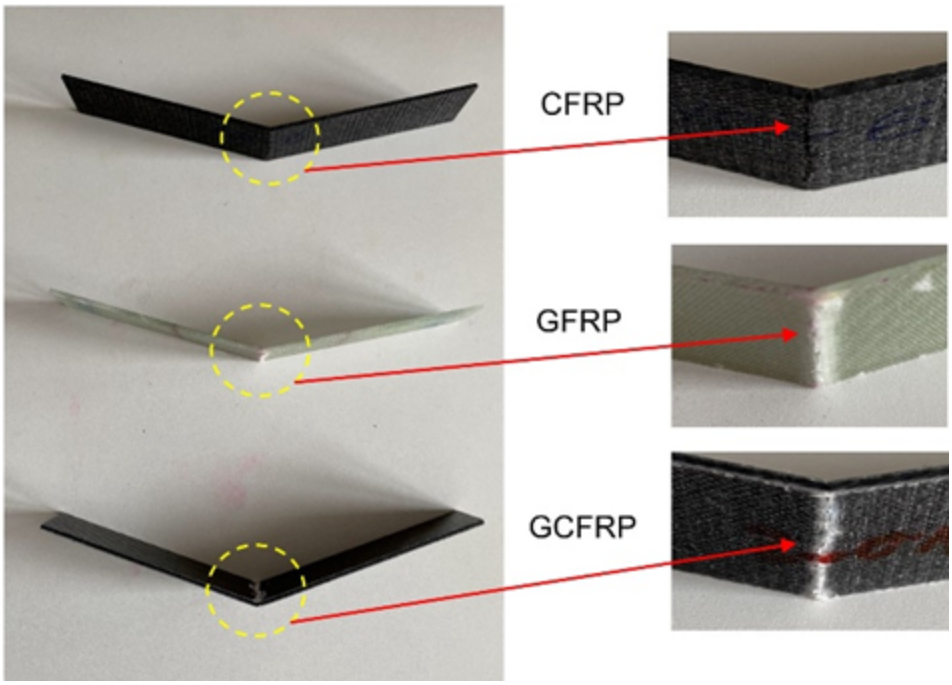

Figure 16

Fracture damage after bending test in CFRP, GFRP and GCFRP composites.

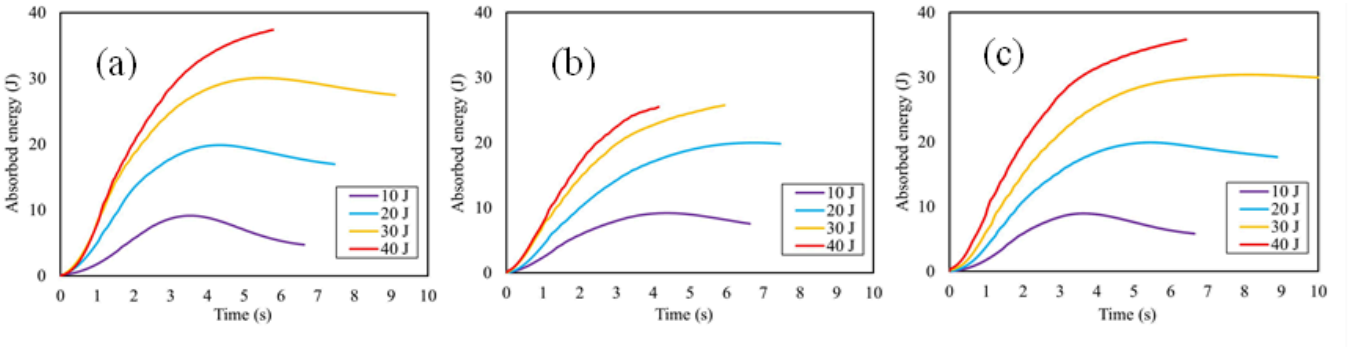

Figure 17

Absorbed energy-time graphs: a) GFRP composites, b) CFRP composites, c) GCFRP composites.

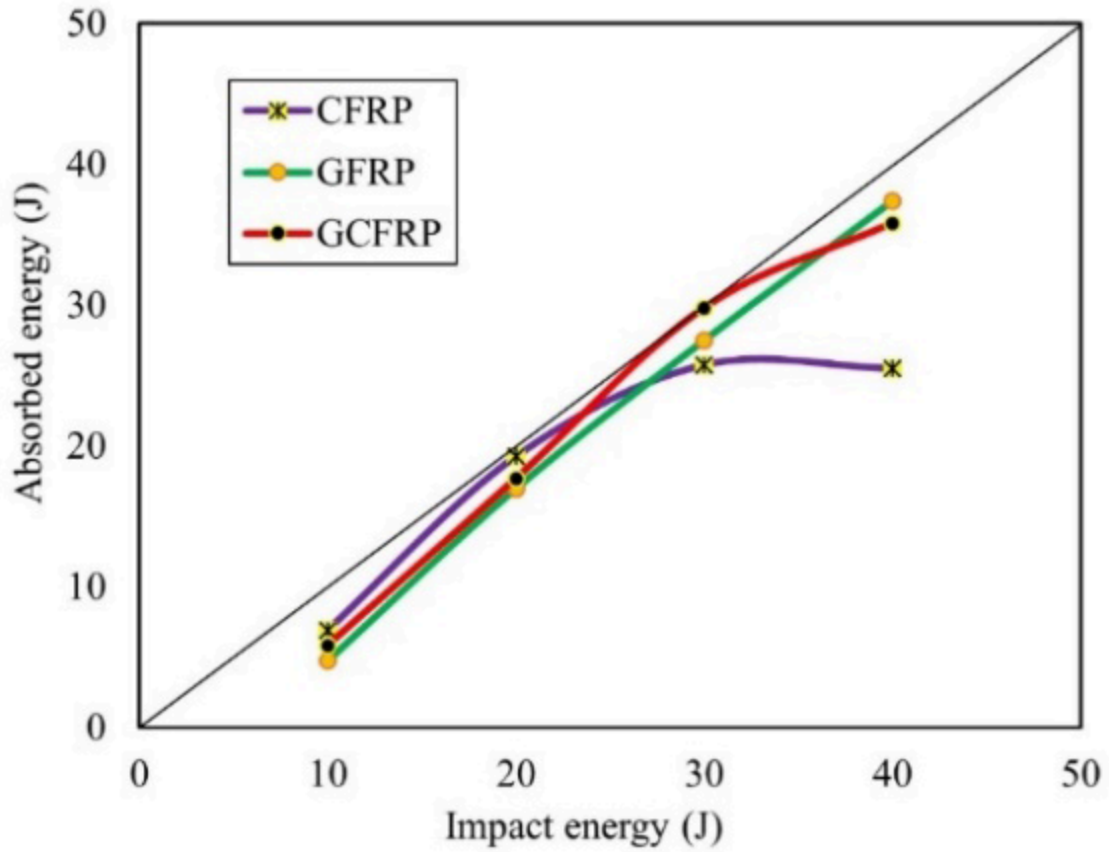

Figure 18

Equal energy diagrams of CFRP, GFRP, and GCFRP.

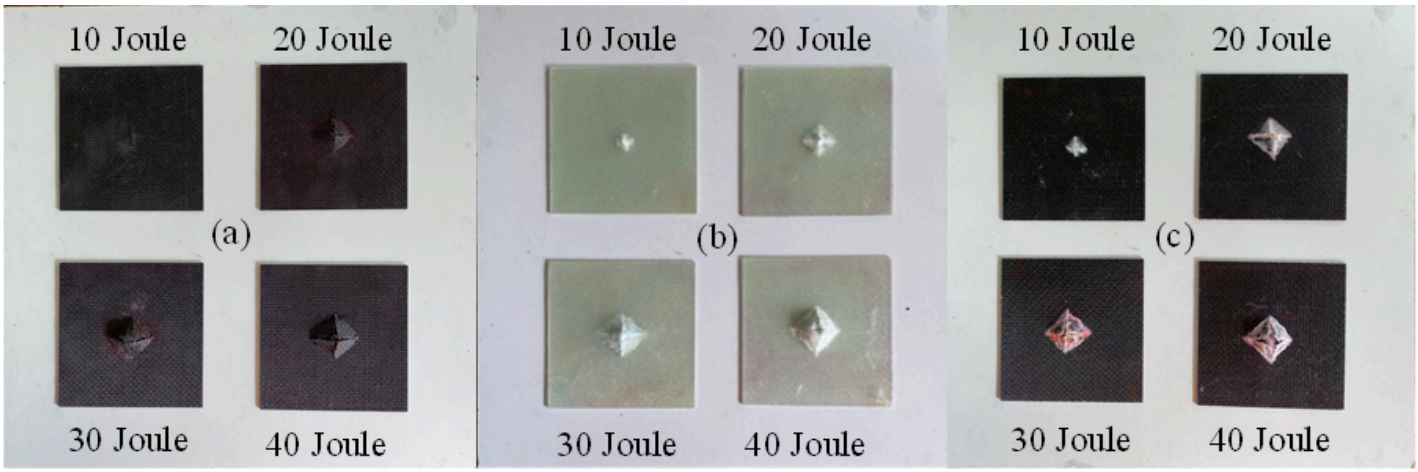

Figure 19

Damages in composites tested at low-velocity impact energies of 10 joules, 20 joules, 30 joules and 40 joules, (a) CFRP, (b) GFRP, (c) GCFRP.

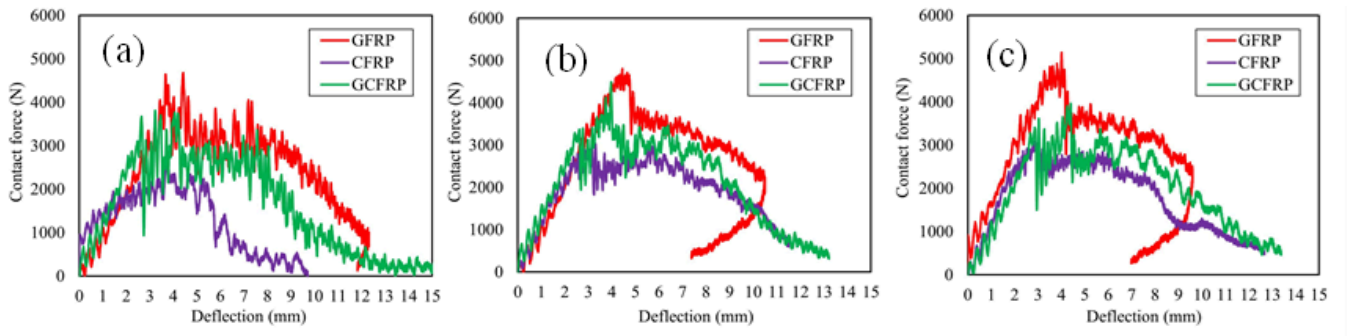

Figure 20

Contact force-deflection graph of GFRP, CFRP and G CFRP composites aged for 90 days at 30 J impact energy; (a) sweater, (b) engine oil, (c) diesel fuel.

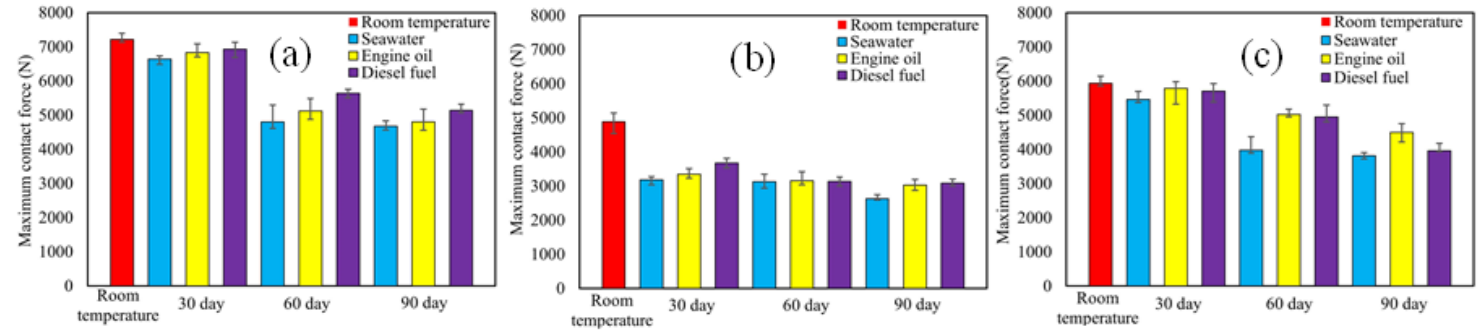

Figure 21

Maximum contact forces of GFRP, CFRP and GCFRP composites to aging environments at 30 J impact energy.

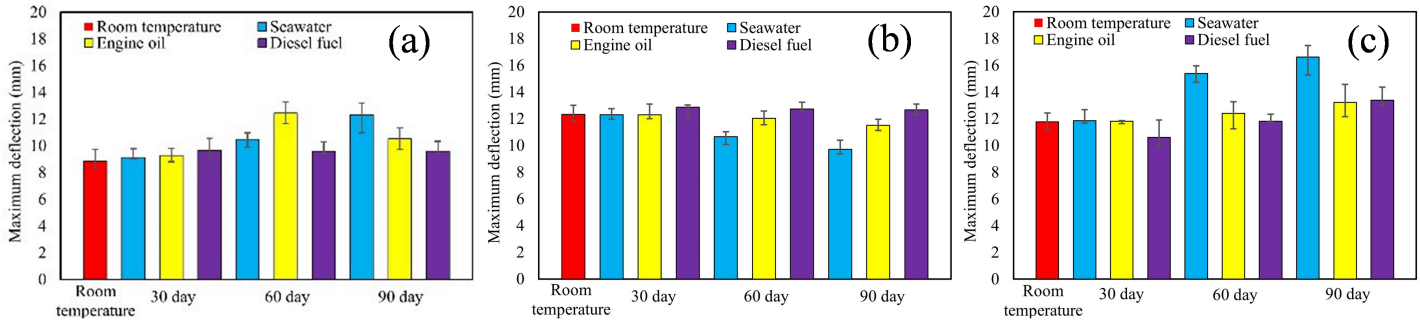

Figure 22

Maximum deflection of GFRP, CFRP and GCFRP composites to aging environments at 30 J impact energy.

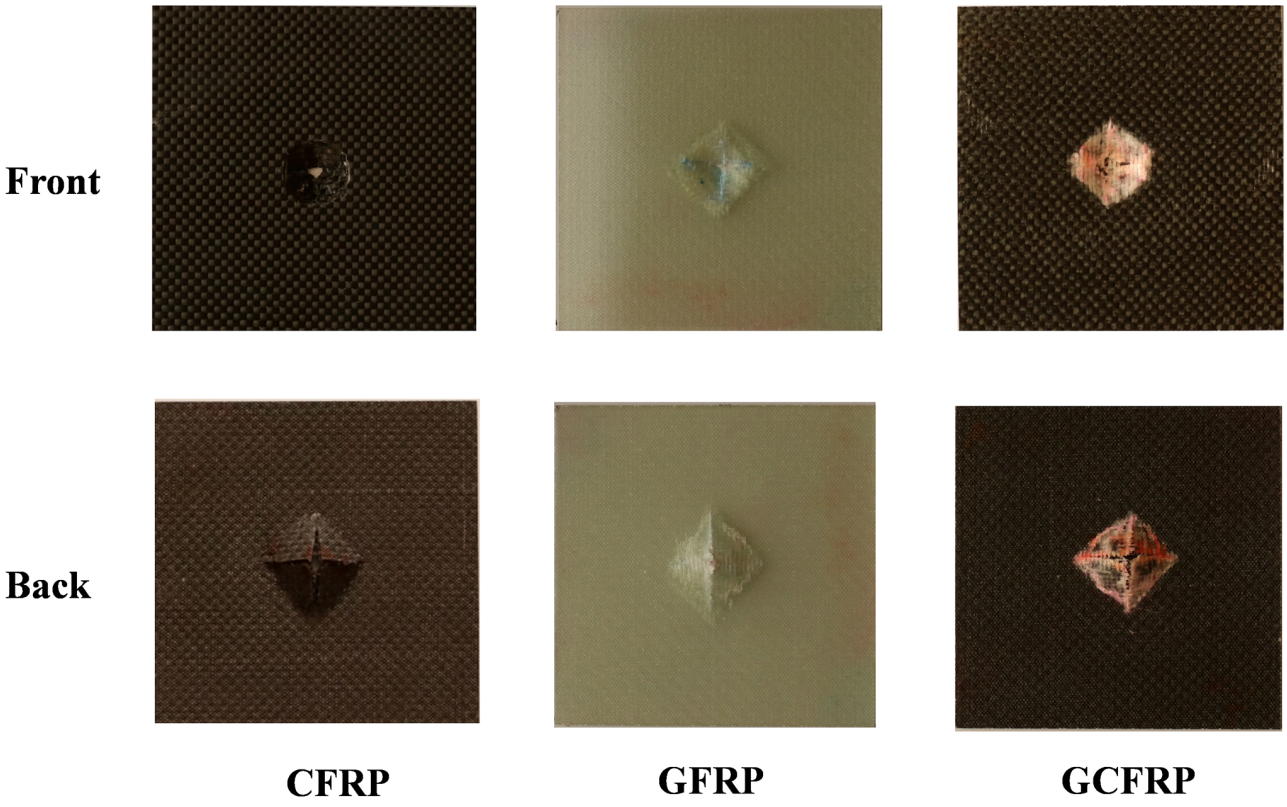

Figure 23

Damages on the front and back surfaces of composites at 30 J impact energy.

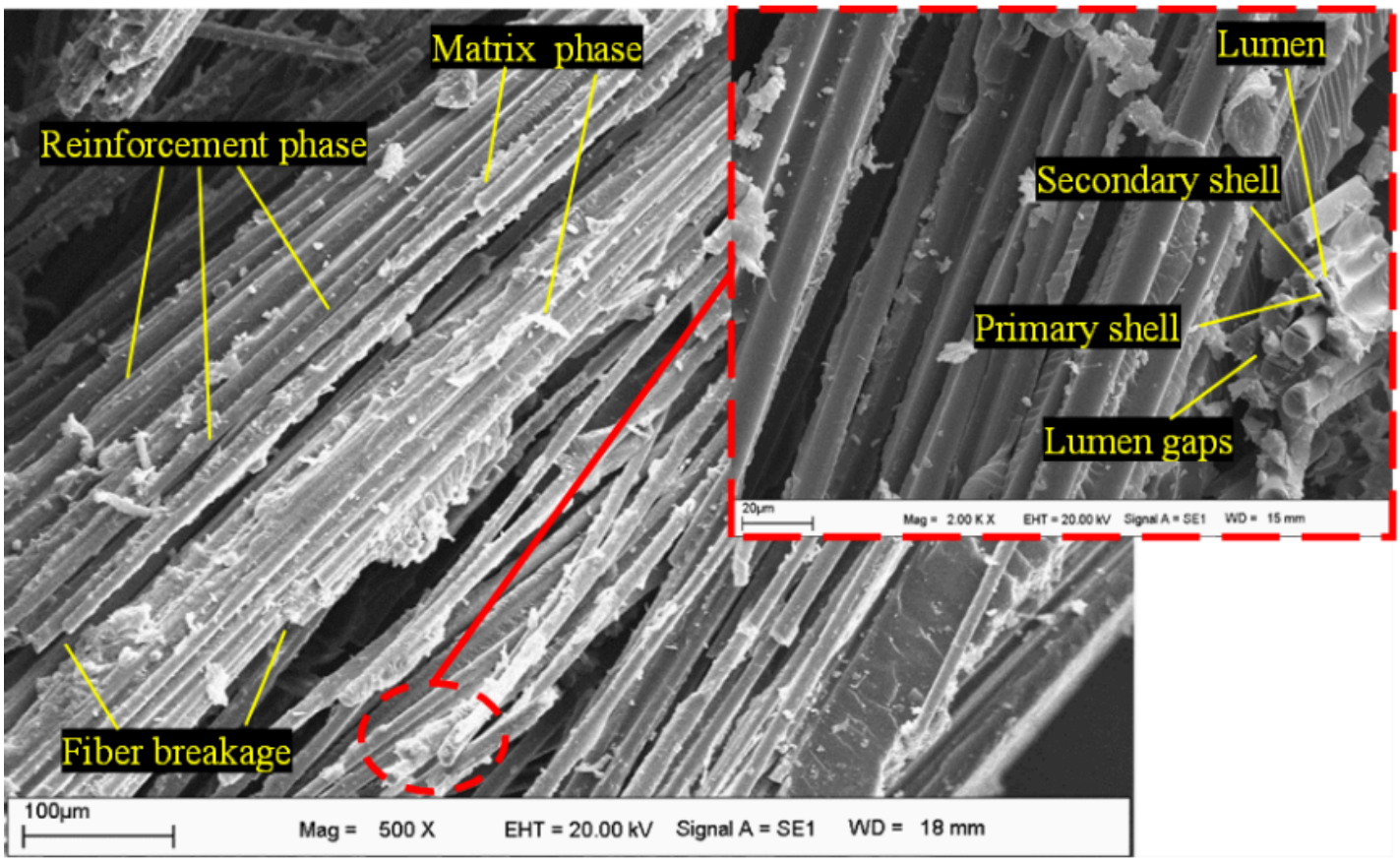

Figure 24

SEM analysis of GFRP composite.

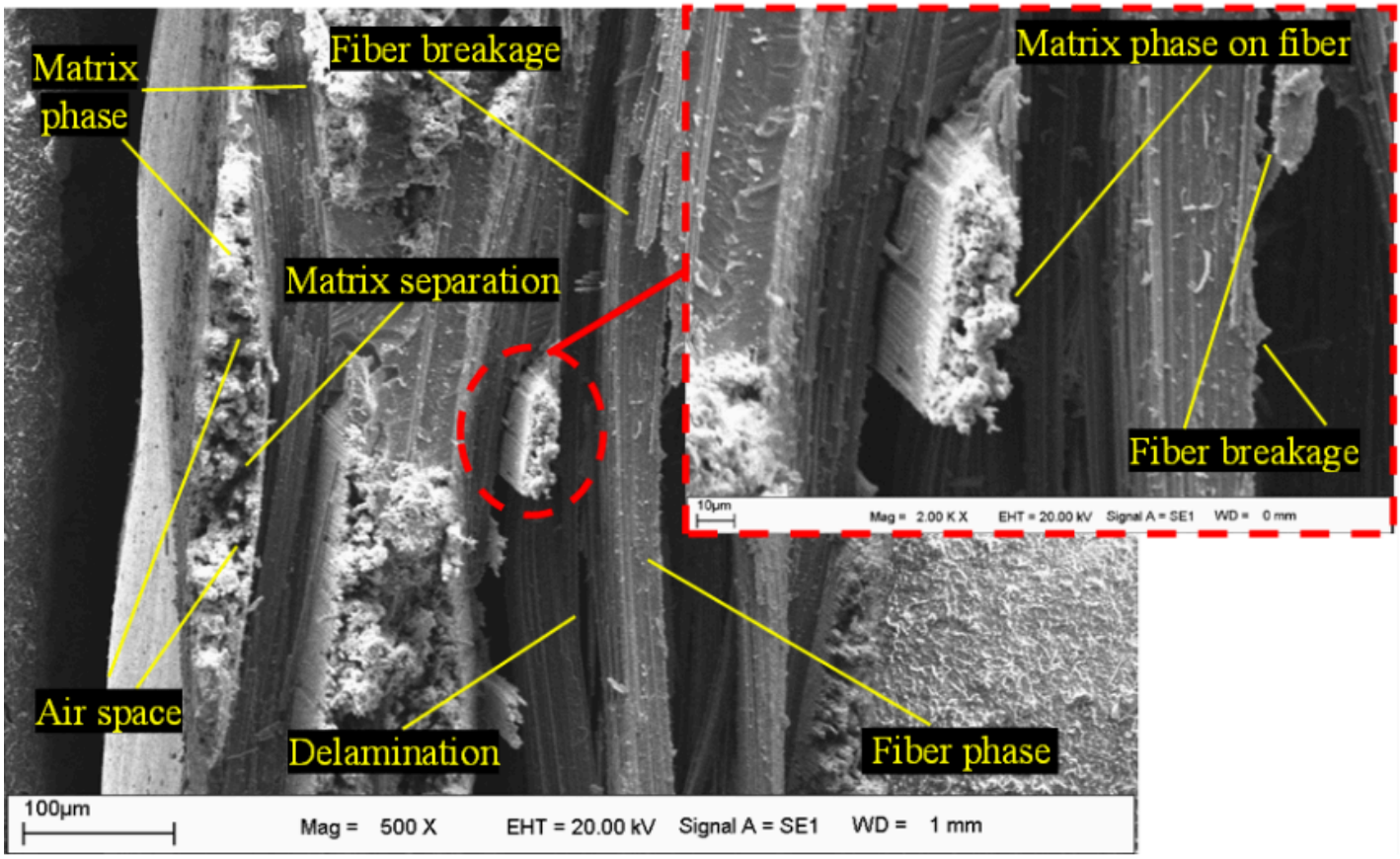

Figure 25

SEM analysis of GFRP composite.

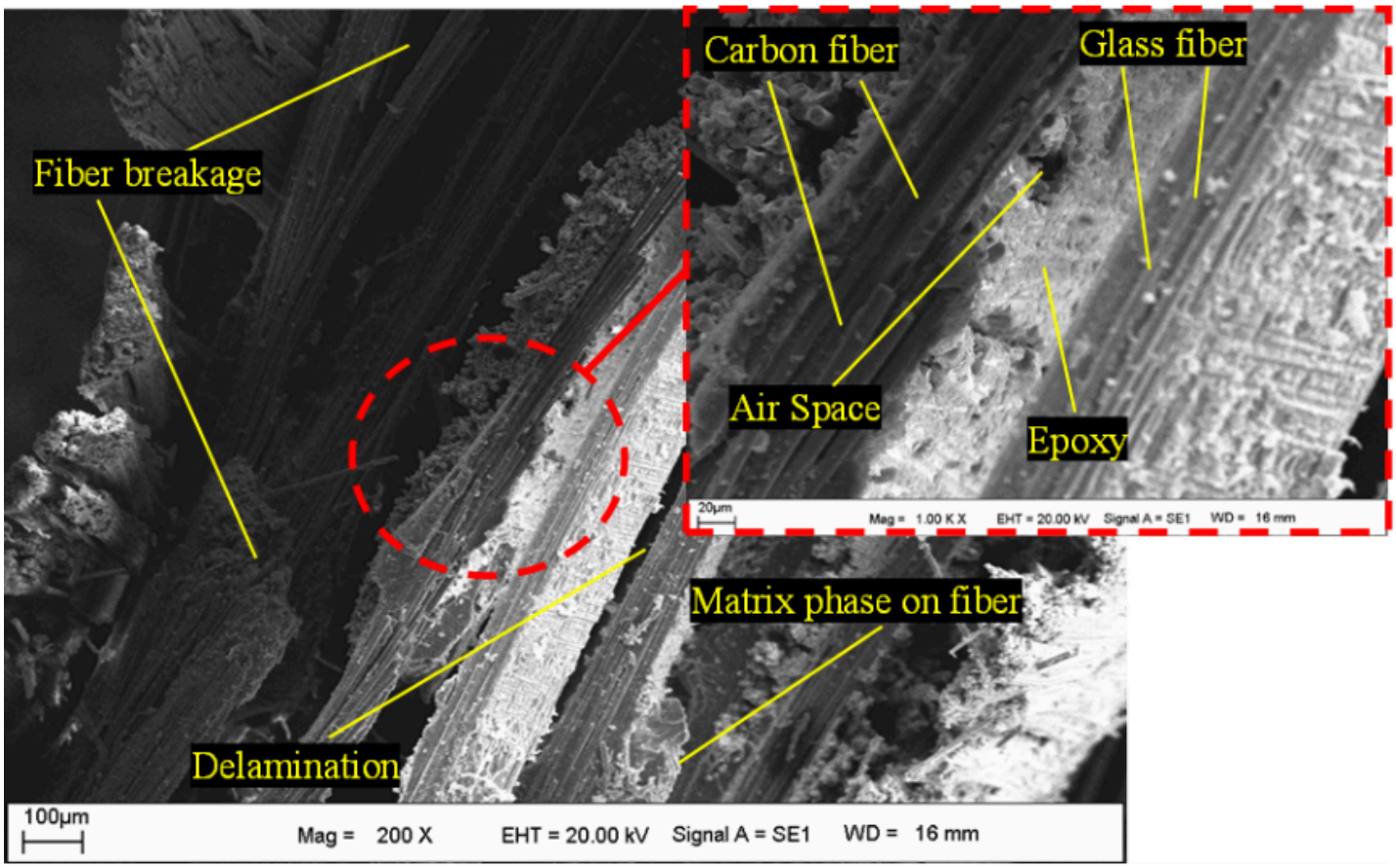

Figure 26

SEM analysis of GCFRP composite.

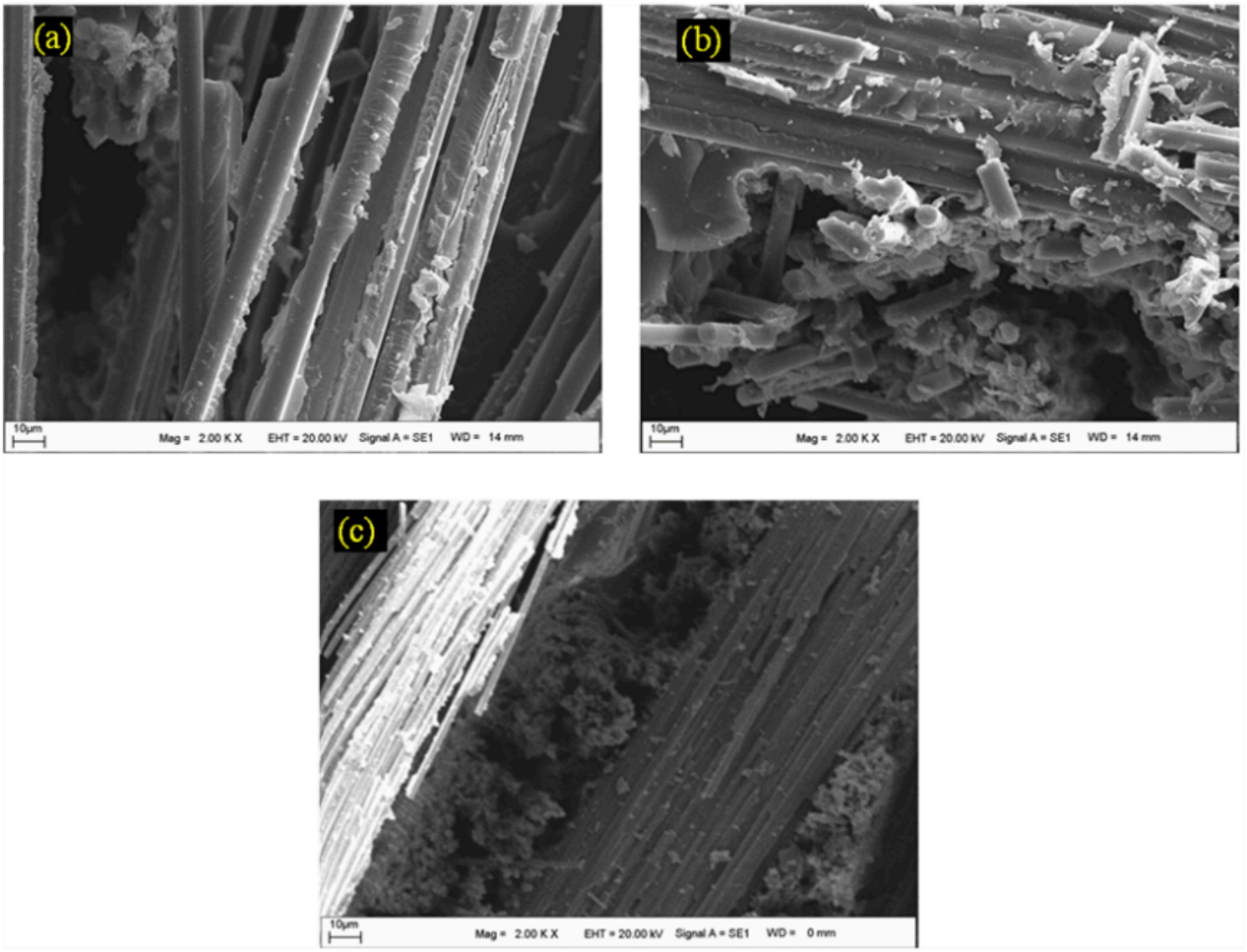

Figure 27

SEM analysis of composites aged for 90 days in seawater; (a) GFRP composites, (b) CFRP composites, (c) GCFRP composites.